AL/CF-TR-1994-0047-Vol. 1

MODELING RESPIRATORY GAS DYNAMICS IN THE AVIATOR'S BREATHING SYSTEM

John B. Bomar, Jr.
Michael W. Scott
Darrin A. Smith

Biodynamic Research Corporation
9901 IH 10 West, Suite 1000
San Antonio, TX 78230

CREW SYSTEMS DIRECTORATE
CREW TECHNOLOGY DIVISION
2504 D Drive, Suite 1
Brooks Air Force Base, TX 78235-5104

May 1994

Final Technical Report for Period May 1993 - December 1993

Approved for public release; distribution is unlimited.

AIR FORCE MATERIEL COMMAND
BROOKS AIR FORCE BASE, TEXAS

NOTICES

This research was conducted under the Small Business Innovation Research (SBIR) Program as a Phase I effort.

Publication of this report does not constitute approval or disapproval of the ideas or findings. It is published in the interest of STINFO exchange.

The U.S. Government does not require SBIR Phase I contractors to adhere to any particular format or style. In accordance with SBIR guidelines for Phase I efforts, the contractor's report is accepted for publication but is not edited.

When Government drawings, specifications, or other data are used for any purpose other than in connection with a definitely Government-related procurement, the United States Government incurs no responsibility or any obligation whatsoever. The fact that the Government may have formulated or in any way supplied the said drawings, specifications, or other data, is not to be regarded by implication, or otherwise in any manner construed, as licensing the holder or any other person or corporation; or as conveying any rights or permission to manufacture, use, or sell any patented invention that may in any way be related thereto.

Customers can obtain a copy of the Appendixes, Volume 2, by writing to the Defense Technical Information Center (DTIC), Building #5, Cameron Station, 5010 Duke Street, Alexandria, VA 22304-6145.

The Office of Public Affairs has reviewed this report, and it is releasable to the National Technical Information Service, where it will be available to the general public, including foreign nationals.

This report has been reviewed and is approved for publication.

Robert B. O'Connor

ROBERT B. O'CONNOR, Captain, USAF
Project Scientist

F. W. Baumgardner

F. WESLEY BAUMGARDNER, Ph.D.
Chief, Systems Research Division

Ronald C. Hill

RONALD C. HILL, Colonel, USAF, BSC
Acting Chief, Crew Technology Division

REPORT DOCUMENTATION PAGE

Form Approved
OMB No. 0704-0188

1. AGENCY USE ONLY *(Leave blank)*	2. REPORT DATE	3. REPORT TYPE AND DATES COVERED
	May 1994	Final May 1993 - December 1993

4. TITLE AND SUBTITLE

Modeling Respiratory Gas Dynamics in the Aviator's Breathing System

5. FUNDING NUMBERS

C - F41624-93-C-6009
PE - 65502F
PR - 3005
TA - CT
WU - 3A

6. AUTHOR(S)

John B. Bomar, Jr.
Michael W. Scott
Darrin A. Smith

7. PERFORMING ORGANIZATION NAME(S) AND ADDRESS(ES)

Biodynamic Research Corporation
9901 IH 10 West, Suite 1000
San Antonio, TX 78230

8. PERFORMING ORGANIZATION REPORT NUMBER

F41624-93-C-6009

9. SPONSORING/MONITORING AGENCY NAME(S) AND ADDRESS(ES)

Armstrong Laboratory (AFMC)
Crew Systems Directorate
Crew Technology Division
2504 D Drive, Suite 1
Brooks Air Force Base, TX 78235-5104

10. SPONSORING/MONITORING AGENCY REPORT NUMBER

AL/CF-TR-1994-0047-Vol. 1

11. SUPPLEMENTARY NOTES

Armstrong Laboratory Technical Monitor: Captain Robert B. O'Connor, (210) 536-3545. This research was conducted under the Small Business Innovation Research (SBIR) program as a Phase I effort.

12a. DISTRIBUTION/AVAILABILITY STATEMENT

Approved for public release; distribution is unlimited.

12b. DISTRIBUTION CODE

13. ABSTRACT *(Maximum 200 words)*

Biodynamic Research Corporation (BRC) completed an SBIR Phase I project to study the feasibility of developing a model of the Aviator's Breathing System (ABS). The motivation for the project was the desire to develop a model which could simulate the cardiovascular and respiratory responses to altitude and acceleration stress encountered in high performance military aircraft. Software modules were developed and tested for simulation of: (1) the flows and pressures within the breathing gas delivery system; (2) the flows, pressures, and gas distribution within the lung; and (3) the steady-state flows and pressures within the cardiovascular system. Subprograms were also developed to compute altitude barometric pressure relationships as well as passenger cabin pressures in military aircraft. In addition to the software development, BRC reviewed and organized the Government furnished data from a series of manned rapid decompression known as the EONS Experiments. The data from approximately 170 experimental decompressions were screened for their suitability for use in parameter selection and validation of the respiratory modeling software. The data appears to be highly coherent and fully usable for model validation. We conclude that the development of an integrated ABS Model is feasible and desirable.

14. SUBJECT TERMS

Aircrew breathing system
Lung mechanics
Mathematical model
Rapid decompression
Respiratory physiology

15. NUMBER OF PAGES

120

16. PRICE CODE

17. SECURITY CLASSIFICATION OF REPORT	18. SECURITY CLASSIFICATION OF THIS PAGE	19. SECURITY CLASSIFICATION OF ABSTRACT	20. LIMITATION OF ABSTRACT
Unclassified	Unclassified	Unclassified	UL

CONTENTS

VOLUME 2 - APPENDIXES

Customers can obtain a copy of the Appendixes, Volume 2, by writing to the Defense Technical Information Center (DTIC), Building #5, Cameron Station, 5010 Duke Street, Alexandria, VA 22304-6145.

FIGURES

TABLES

ACKNOWLEDGMENTS

The members of the research team express their deep appreciation to the many individuals making contributions to this research program. Without the timely assistance given so generously by everyone, this research program and this report could not possibly have been accomplished.

A special thanks is given to Captain Robert B. O'Connor as the USAF Project Scientist in the Crew Systems Directorate, Armstrong Laboratory, Human Systems Division, for his support, management and leadership during this research program.

Finally, the research team gives a very special thank you to the management and support staff at BRC. Without the efforts of Ms. Karen Lindley, the editing and publication of this research program could not have been accomplished effectively. Appreciation is also given to Mr. John Martini for the illustration support, to Ms. Patricia Perret for the technical library support, and to Mr. Thomas Kingery for contract management.

SECTION 1.0

1.0 Summary.

Biodynamic Research Corporation (BRC) completed an SBIR Phase I project to study the feasibility of developing a model of the Aviator's Breathing System (ABS). The motivation for the project was the desire to develop a model which could simulate the cardiovascular and respiratory responses to altitude and acceleration stress encountered in high performance military aircraft. Once validated, the model could be employed to integrate existing physiologic knowledge and to estimate the physiologic effects of changes in the environment or the design of aircrew protective equipment.

The Phase I effort was concentrated in developing computer software modules which were capable of simulating the main effects of environmental variables on the breathing system hardware and respiratory and cardiovascular systems. Software modules were developed and tested for simulation of: (1) the flows and pressures within the breathing gas delivery system; (2) the flows, pressures, and respiratory gas distribution within the lung; and (3) the steady-state flows and pressures within the cardiovascular system. Subprograms were also developed to compute altitude-barometric pressure relationships as well as passenger cabin pressures in military aircraft.

In addition to the software development, BRC reviewed and organized the Government furnished data from a series of manned rapid decompressions known as the "EONS Experiments." The data from approximately 170 experimental decompressions were screened for their suitability for use in parameter selection and validation of the respiratory modelling software. The data appears to be highly coherent and fully usable for model validation. The summarized results of the EONS Experiments represent new physiologic database which is directly applicable to USAF operational scenarios. The respiratory gas composition time histories represent original scientific data suitable for publication and use by the aerospace medicine community independently of their value in the ABS modelling effort.

The work accomplished in Phase I has laid the groundwork for developing an integrated ABS Model in a Phase II SBIR program. BRC has written prototype software modules which form the major building blocks for the Phase II ABS Model. We conclude that the development of an integrated ABS Model is feasible and desirable. We also conclude that there is sufficient existing data for selection of parameters and independent validation of the major components of the Phase II ABS model. However, the complete validation of the combined effects of acceleration, pressure breathing and altitude on the ABS must await new experimental data. Fortunately, the attempt to simulate the physiologic response to combined stressors will explicitly point to missing data and guide the development of experimental protocols to elucidate their significance.

SECTION 2.0

2.0 Introduction.

This final report concludes an effort by Biodynamic Research Corporation (BRC) of San Antonio, Texas to conduct a study to investigate the feasibility of creating a computer model of the respiratory gas dynamics in the military aviator's breathing system. The work was conducted under Contract #F41624-93-C-6009 through the Armstrong Laboratory and is entitled "Modelling Respiratory Gas Dynamics in the Aviator's Breathing System."

The aim of the study was to establish the feasibility of creating a comprehensive mathematical model of the Aviator's Breathing System (ABS) which could be employed to simulate the dynamics of respiratory gas movement and exchange in breathing systems for high performance military aircraft. The ABS Model could be employed as a tool for integrating existing physiologic knowledge and for guiding future research by explicitly identifying the new data required to more fully describe the physiologic consequences of breathing system design, as well as assist in elucidating the major effects of the environment and protective systems on aircrew performance, safety, and comfort. The major technical objectives of the Phase I project are listed below:

(1) Conduct a review of the literature to assess previous models for their suitability as components of the ABS model and to glean physiologic data from the literature for use in parameter identification and model validation.

(2) Synthesize mathematical models of the components of the Aviator's Breathing System including: pulmonary mechanics and gas exchange, cardiopulmonary gas transport, and parametric models of oxygen delivery system components.

(3) Analysis of Government furnished experimental rapid decompression data.

(4) Develop model parameters and partially validate tentative models of the ABS components.

(5) Assess the feasibility of development of a comprehensive ABS model in Phase II.

Biodynamic Research Corporation performed all of the analysis for this contract. This final report documents the work generally according to the objectives listed above. Section 3 provides general background on modelling and simulation of relevant physiologic systems and breathing system components. Sections 4 through 6 discuss the component system models separately and give additional background and technical details. Section 7 presents the analysis of the Government furnished experimental data which is summarized in Appendix A. Finally, Section 8 presents conclusions and recommendations together with the assessment of the feasibility of creating a comprehensive integrated ABS Model in Phase II. In addition to the experimental data summary, the appendices to this report contain a comprehensive bibliography of relevant literature and the listings of the computer programs developed during the project.

SECTION 3.0

3.0 Technical Background and Literature Review.

3.1 Modelling Oxygen Delivery Systems.

There are ample laboratory data describing the flow/pressure relationships within breathing systems.[1,2,3,4,5,6,7] However, other than the present project, the authors are not aware of any attempts to model USAF breathing gas delivery systems. There is one report that describes a model of a simple US Navy demand regulator, but no details of the system equations were given.[8] The breathing system model created during the present study simulates the pressures and flows in a generic oronasal mask during breathing through a diluter-demand breathing regulator.

Because breathing regulators are inherently nonlinear devices, writing and solving models of their function is difficult. One alternative method of modelling regulators is to characterize their performance parametrically over the operating range of interest. With the exception of the Navy study cited above, parametric modelling of empirical data has invariably been used for describing regulator performance. A more rigorous, but much more difficult method is to write and solve the system equations for the regulator of interest. For the Phase I ABS study, the regulator was modelled parametrically, while the oronasal mask was modelled by solving the system equations describing its performance.

3.2 Modelling Respiratory Function.

Models of steady state respiratory gas exchange are well established.[9] The most commonly employed of these is the Alveolar Gas Equation (AGE)[10] which describes the steady state relationship between barometric pressure, fraction of inspired oxygen, and the fractions of oxygen and carbon dioxide in the alveoli. Although useful in many aerospace applications, the AGE cannot describe the breath-to-breath transients which occur during ordinary breathing, nor can it be employed to describe the dynamics of respiratory gas exchange during rapid changes in ambient pressure or when there is a net exchange of nitrogen between the lung and the environment. During most flight operations, even at high altitudes, as long as the aircraft cabin pressurization system remains functional, the AGE may be employed to set the breathing system design criteria for avoiding undue hypoxia. However, during rapid changes in cabin altitude and/or changes in the pressure or composition of the inspired breathing gas, the assumptions required for use of the AGE are violated. Thus, there will be significant errors between the actual alveolar gas composition and that predicted by the AGE until the respiratory steady state is re-established.

To adequately describe breath-by-breath gas dynamics in the lung during pressure/ composition transients, a model which includes the spatial and temporal variation of ventilation and perfusion within the lung is required. There are several models described in the literature which describe cardiopulmonary function in clinically significant pulmonary disease or for teaching respiratory physiology.[11,12,13,14,15,16,17] Unfortunately, these were developed for modelling a particular physiologic response or for a particular

Figure 3-1. Aviator's Breathing System

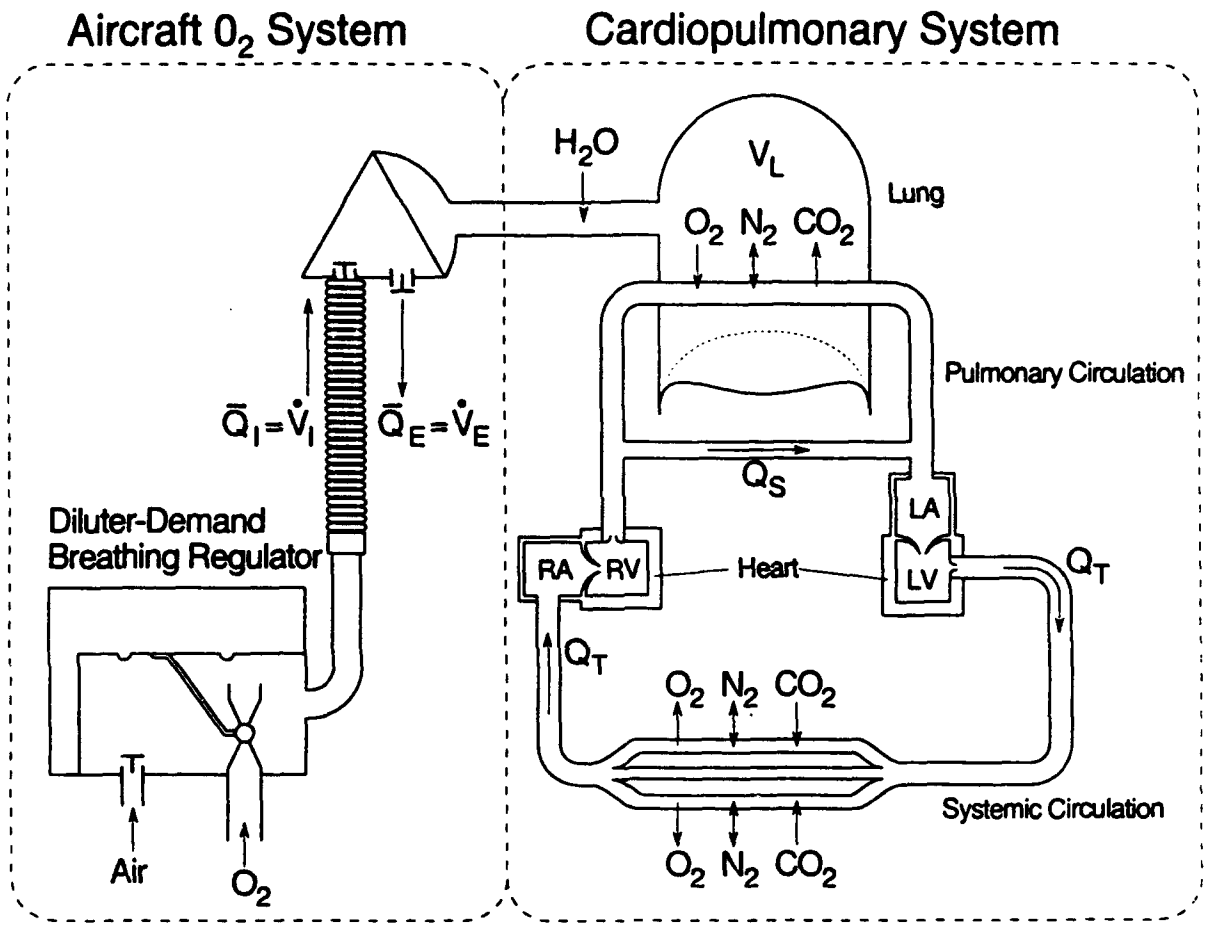

environment or clinical situation. For the most part, previous models are not easily adaptable to the high performance aviation scenario because they do not describe many of the relationships between the environment, the breathing system, and the crew member's other protective systems. As an alternative, BRC proposed the development of an ABS model tailored to model the gas flows and composition within the breathing and respiratory systems in typical operational and experimental environments encountered by military aircrews.

For the ABS Phase I project, two modules were developed which together describe the vertical ventilation pattern in the lungs and the concentration of a tracer gas throughout the lungs during inspiration and expiration. The lung is modelled as four regions of equal mass that are located along the vertical axis of the lung. The model accounts for the volume and ventilation differences created by gravity, which have traditionally been called "interregional differences" by physiologists. A detailed description of the ABS Phase I models is given in Section 5.0.

3.3 Modelling the Cardiovascular System.

Ultimately, the ABS model seeks to describe the cardiopulmonary physiology associated with the various environmental stressors associated with high performance flying. Early in the Phase I program, it became apparent that a reasonably complete model of the cardiovascular system would be required to adequately model the effects of positive pressure breathing (PPB) for altitude and acceleration protection (PBA and PBG). Thus, it was decided to create a steady state cardiovascular model for the Phase I program which could be extended to a dynamic model in Phase II. We concentrated our literature search on modern cardiovascular modelling work which appeared to be sufficiently comprehensive, but not overly complicated. In particular the cardiovascular model described in Section 6.0 parallels the developments presented in a paper by White, et al.[18] It also draws from papers by Jaron, et al.,[19,20,21] whose approach was similar to that presented in earlier papers by Rideout,[22] Snyder,[23] and Avula.[24] All of these authors cited the earlier work of Womersley[25] who developed equations describing the convection of fluids in elastic tubes as well as those describing the propagation of pressure waves and pressure dependent changes in tube radius.

3.4 Integrated Models of Cardiopulmonary Function.

The authors are aware of only one integrated model of the physiologic function of the human body, a computer model known as Human[26]. Human is a teaching program for medical students which is an integrated computer model of the entire body. BRC has experience with an old version and has been impressed with its fidelity, given its simplicity. BRC has purchased the source code for Human and has working versions written in both MS-DOS Fortran and MS-DOS Quick Basic (QBX). The general approach employed in Human is to model physiologic function by use of curve fits to empirical data. This approach limits Human's use to conditions which have been incorporated in the model. Unfortunately, Human as presently configured only allows small excursions from sea level, +1 Gz conditions. However, the approach employed in Human to implement physiologic control systems, such as the baroreceptor system for control of cardiac output, is simple and effective. It is suggested that a similar approach can be employed to model the physiologic feedback control in the Phase II ABS model. It would be relatively straightforward to refine and modify the Human code to simulate the range of conditions required for the ABS model.

3.5 Modelling the Environment.

By the environment, we mean the physical environment including such things as the barometric pressure, the temperature, the acceleration, etc. Most environmental variables would be implemented as inputs to the hardware and physiologic models. The Phase I ABS Model includes subroutines which model the variation in atmospheric pressure with altitude as well as the change in MILSPEC cabin pressure with altitude. Both models are included as part of the model of the regulator and oronasal mask described in Section 4.0.

3.6 Summary.

At the present time, there are no comprehensive physiologic models which can describe the physiologic consequences of changes in operating conditions and design of the Life Support Systems (LSS) employed in modern high performance aircraft. BRC has created tentative computer models of the components required to implement an integrated model of the ABS which simulates the function of the hardware and the physiologic subsystems in response to environmental changes. Detailed description of the newly developed models are given below with comments on the improvements necessary to create an integrated ABS Model in a Phase II SBIR program.

SECTION 4.0

4.0 Mask and Regulator Models.

4.1 General Description.

The mask and regulator models simulate the time varying flows and pressures within breathing system from the regulator outlet to the trachea during the breathing cycle. Both models are based on the performance standards promulgated by the Air Standardization and Coordinating Committee in Air Standard 61/21.[27]

4.2 Mask Model.

The mask is modelled as a dead space and two variable area orifices through which inspiratory and expiratory flows separately pass. The inspiratory valve model relates the flow and pressures between the mask supply hose and the oronasal cavity during inspiration. The expiratory valve model relates the flow and pressure drop between the mask cavity and the external ambient atmosphere during expiratory flow. Both valve models are based on empirical data collected on the RAF P/Q mask,[28] which meets the Air Standardization Coordinating Committee flow resistance standards.[27] Other valve models can be substituted. The general form of the model is

$$\dot{V} = f(A_{valve}, \Delta P_{valve}) \quad . \qquad [4\text{-}1]$$

where, A_{valve}, is the mask valve area, $\dot{V}_{valve}$ is the instantaneous volume flow through the valve. The model actually calculates the mass flow through the valves and converts the result to volume flow using the gas composition and the prevailing temperature and absolute pressure. The valve area, A_{valve}, is in turn a function of the pressure drop, ΔP_{valve}, across the valve. The valve models are solved by estimating the area of the valve from the current pressure conditions and then computing the flow through the valve using ideal orifice equations. Mask leaks can be modelled by parallel flow paths to ambient, but none are included in the present model. Expiratory valve compensation is simulated by adding any positive difference between mask hose pressure and ambient pressure to the expiratory valve down stream pressure. In the absence of compensation, the down stream pressure for the expiratory valve is ambient atmospheric absolute pressure plus the valve cracking pressure.

The mask hose and connectors are modelled as simple tubes with flow-pressure drop relationships based on quadratic fits to typical data. Data describing specific actual equipment can be substituted.

4.3 Regulator Model.

The authors know of no published functional models of modern breathing regulators. There is one report that describes a model of a simple US Navy demand regulator, but no details of the system equations were given.[8] Transfer function models of breathing regulators have

also been employed to investigate regulator stability.[9] However, breathing regulators are inherently nonlinear devices, so that a transfer function approach can only accurately model regulator function over a limited range of operating conditions. Therefore, we chose to simulate the performance of an ASCC regulator rather than its function. The regulator is simulated parametrically as a mass flow into the distal end of the mask tube in response to pressure changes at the regulator outlet. Pressure Breathing for Altitude (PBA) or for high acceleration (PBG) are accommodated by a regulator outlet reference pressure which can be made a function of ambient pressure or acceleration. The outlet gas composition may be included in the simulation to duplicate the regulator dilution performance for various environmental conditions. The Phase II regulator model(s) can be modified to represent the specific performance of any breathing regulator for which empirical flow-pressure data are available.

4.4 Airway Resistances.

In the mask model, airway resistances are modeled by simple quadratic fits to physiologic data. The resistance of the bronchi and trachea are included in the model, as is the pressure loss in the oronasal cavity. The intrapulmonary pressures estimated in the Mask Model represent the mean pressure at the entrance to the alveolar space. The Pulmonary models described in Section 5.0 compute the regional intrapulmonary pressures more accurately than the technique employed here. The Phase II ABS model will integrate the mask and pulmonary models and will employ the more accurate methods described in Section 5.0, but simple models were included in the Phase I Mask Model in the interest of completeness.

In the Mask Model, the resistances for mouth breathing and nose breathing are accounted for separately. The following empirical model[29] is employed.

$$\Delta P = K_1 \cdot \dot{V} + K_2 \cdot \dot{V}^2 \quad . \qquad [4\text{-}2]$$

The values for the K's were also taken from reference 29. For mouth breathing,

$K_1 = 2.35 \cdot 10^5$ Pa·sec·m^{-3} and $K_2 = 2.94 \cdot 10^7$ Pa·sec·m^{-6}.

For the nose breathing there are separate K_2's for inspiration and expiration, but K_1 is the same for both phases.

$K_1 = 2.94 \cdot 10^5$ Pa·sec·m^{-3}, and

Inspiratory $K_2 = 2.94 \cdot 10^8$ Pa·sec·m^{-6}, and

Expiratory $K_2 = 3.92 \cdot 10^8$ Pa·sec·m^{-6}.

The overall pressure drop is modelled by assigning the relative fraction of the total breathing flow to the mouth and nose, respectively. The individual drops are weighted by the flow fractions. Thus,

$$F_m + F_n = 1 \ , \qquad [4\text{-}3]$$

and

$$\Delta P_{Airway} = F_m \cdot \Delta P_{mouth} + F_n \cdot \Delta P_{nose} \ . \qquad [4\text{-}4]$$

4.5 Forcing Function.

The Phase II ABS Model will employ the Pulmonary Model to generate mask flows in response to differences in intrapleural pressure and external pressures on the thorax and abdomen. For the present, we employed a simple sinusoidal forcing function for the Mask Model to simulate the volume change generated by the lung during breathing. The present coding models the lung volume change by the following function.

$$V_L(t) = V_{RC}(P_{pl}) - \frac{\dot{V}_{L_{max}}}{\omega} \cdot Cos(\omega t) \ , \qquad [4\text{-}5]$$

so that the lung flow is

$$\dot{V}_L = \dot{V}_{L_{max}} \cdot Sin(\omega t) \ . \qquad [4\text{-}6]$$

4.6 Simulation Results.

To demonstrate the model output, system flows and pressures were computed for moderate breathing at ground level. The respiration rate was 20 breaths·min^{-1}, the tidal volume was 1.5 L, and the peak inspiratory flow was 94.2 L·min^{-1}. Figure 4-1 shows the system flows for the regulator, mask, and lung. Positive flows are into the mask and lung (and out of the regulator), while negative flows are flows out of the mask and lung. An inter-breath pause is simulated by a short period between cycles during which there is no flow. The flows in the mask and lung are computed at Body Temperature and Pressure, Saturated (BTPS) conditions, while the flow from the regulator outle ,, rough the mask tube are computed at Ambient Temperature and Pressure, Dry (ATPD) conditions. The mask and lung flows are virtually identical, so that their curves are superimposed in the plot. Figure 4-2 illustrates the system pressures on both absolute and differential pressure scales. The pressures correspond to the flows shown in Figure 4-1. Thus, the minimum pressures correspond to

Figure 4-1. System Flows for the Regulator, Mask, and Lung

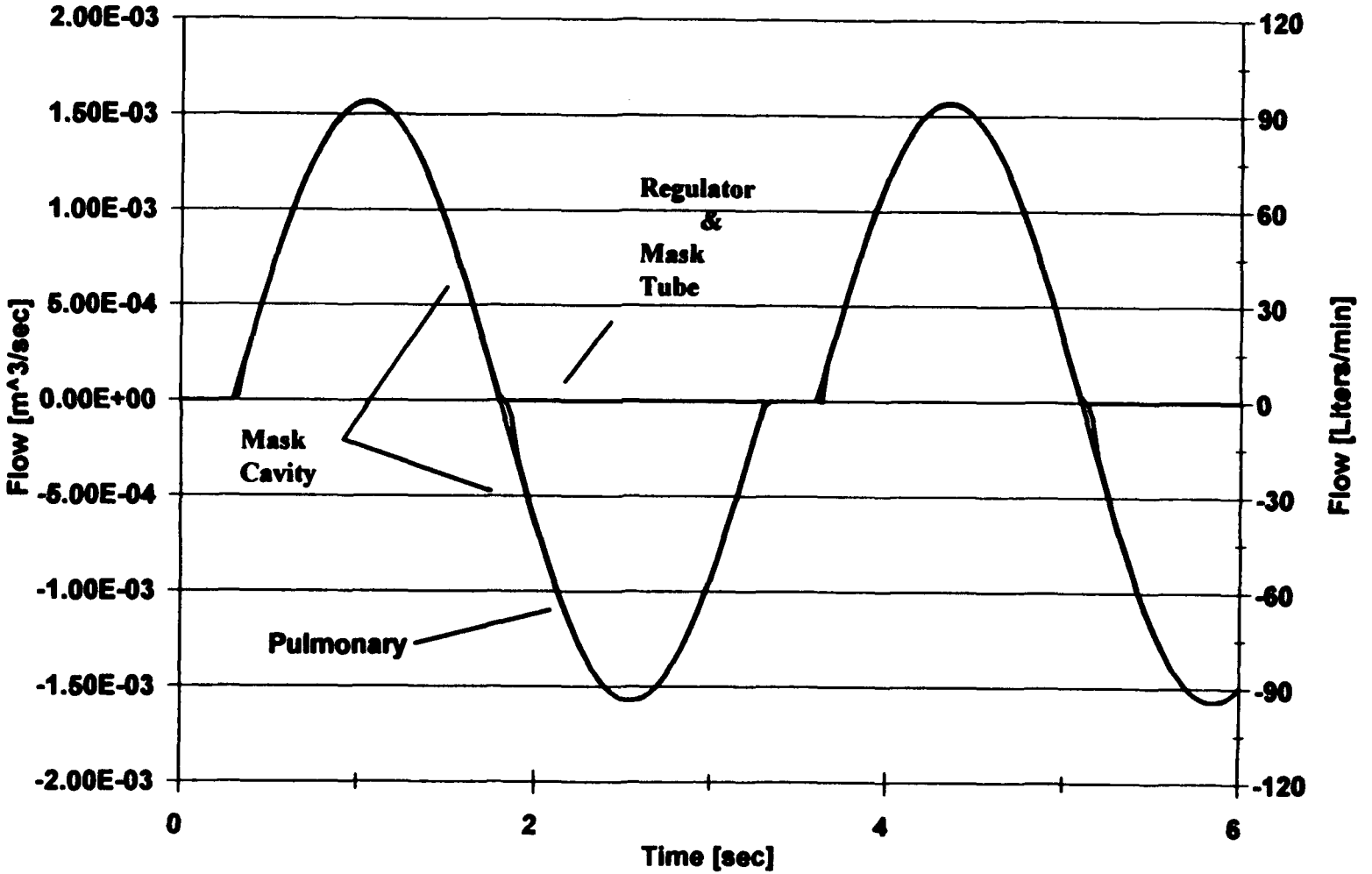

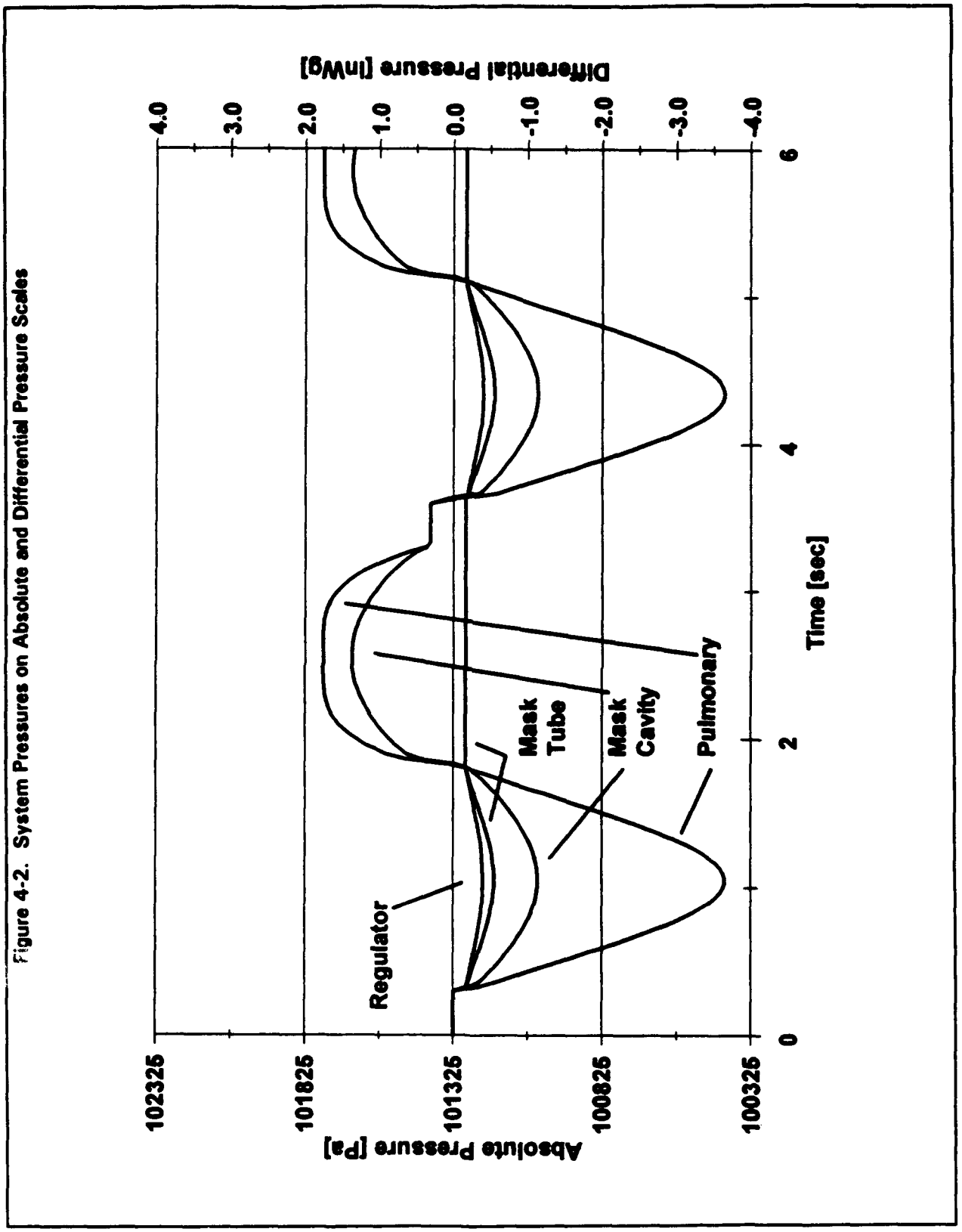

Figure 4-2. System Pressures on Absolute and Differential Pressure Scales

the peak inspiratory flows, while the maximum pressures correspond to the peak expiratory flows. Figure 4-3 shows the system volumes (cumulative flows). As shown, the flows into and out of the mask and lung are equal for a single cycle of the sinusoidal breathing pattern. Thus, the mask and lung volumes rise and fall around their initial values. Since the regulator flow is unidirectional, the volume increases during each inspiratory cycle and remains constant during the expiratory cycles.

The model's ability to simulate a rapid decompression is illustrated in Figures 4-4, 4-5, and 4-6. Figure 4-4 displays the system absolute pressures during a 5 psig (3.45 kPa) decompression from sea level to 11,000 feet (3353 m) altitude. The differential pressures are given in Figure 4-5. The "breathing" in the model was paused during the 1.65 sec rapid decompression. The model contains a simulated relief valve which controls the regulator outlet and mask tube pressure. As implemented, the relief is ideal. That is, it has no flow resistance. Thus, the mask cavity pressure rise is limited during the simulated decompression. The Phase II regulator model will include code to simulate the function of an actual compensated poppit relief which will give a more realistic response to pressure changes. Figure 4-6 shows the system flows corresponding to the pressure transients in Figure 4-5.

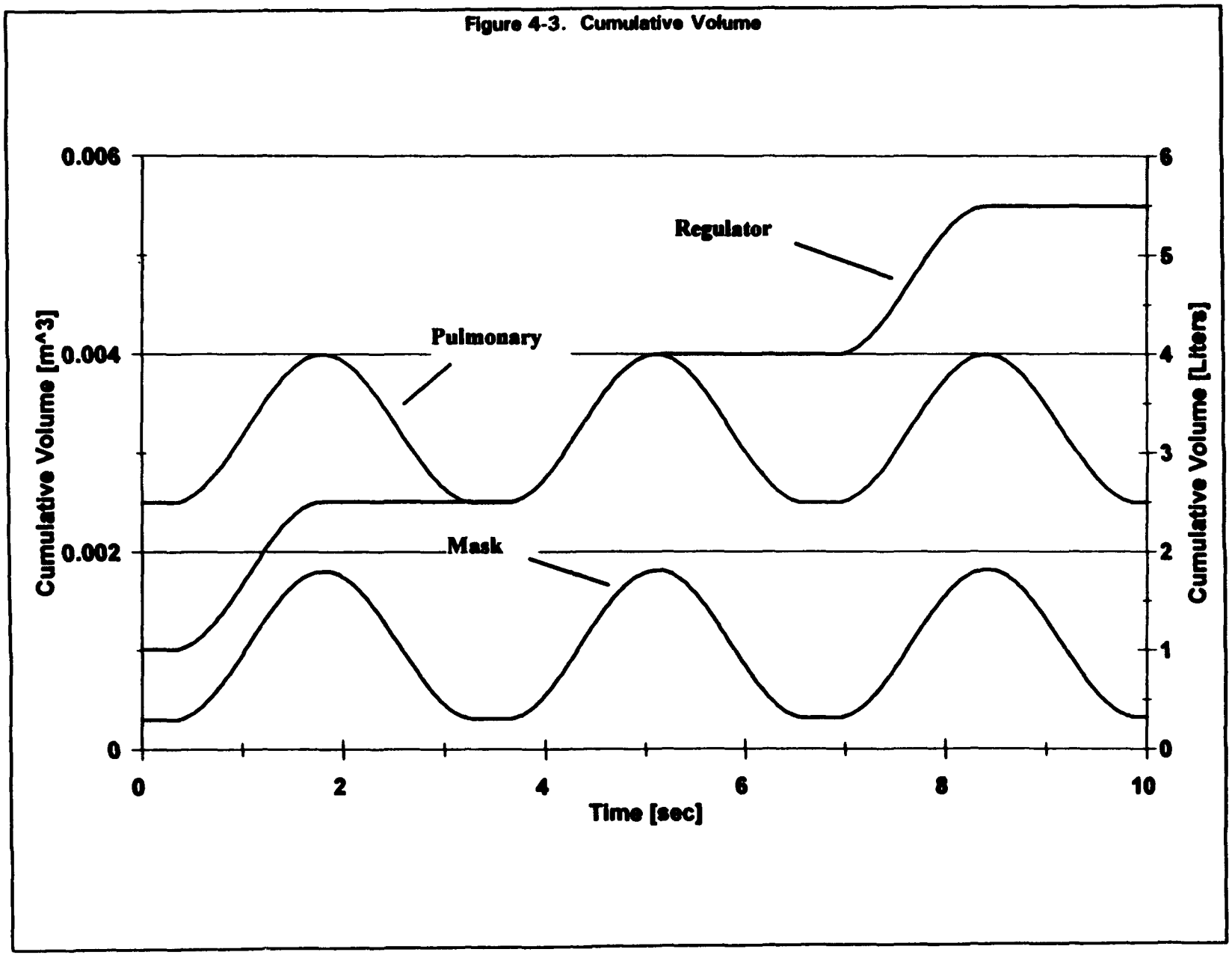

Figure 4-3. Cumulative Volume

Figure 4-4. System Absolute Pressures During a 5 psig Decompression

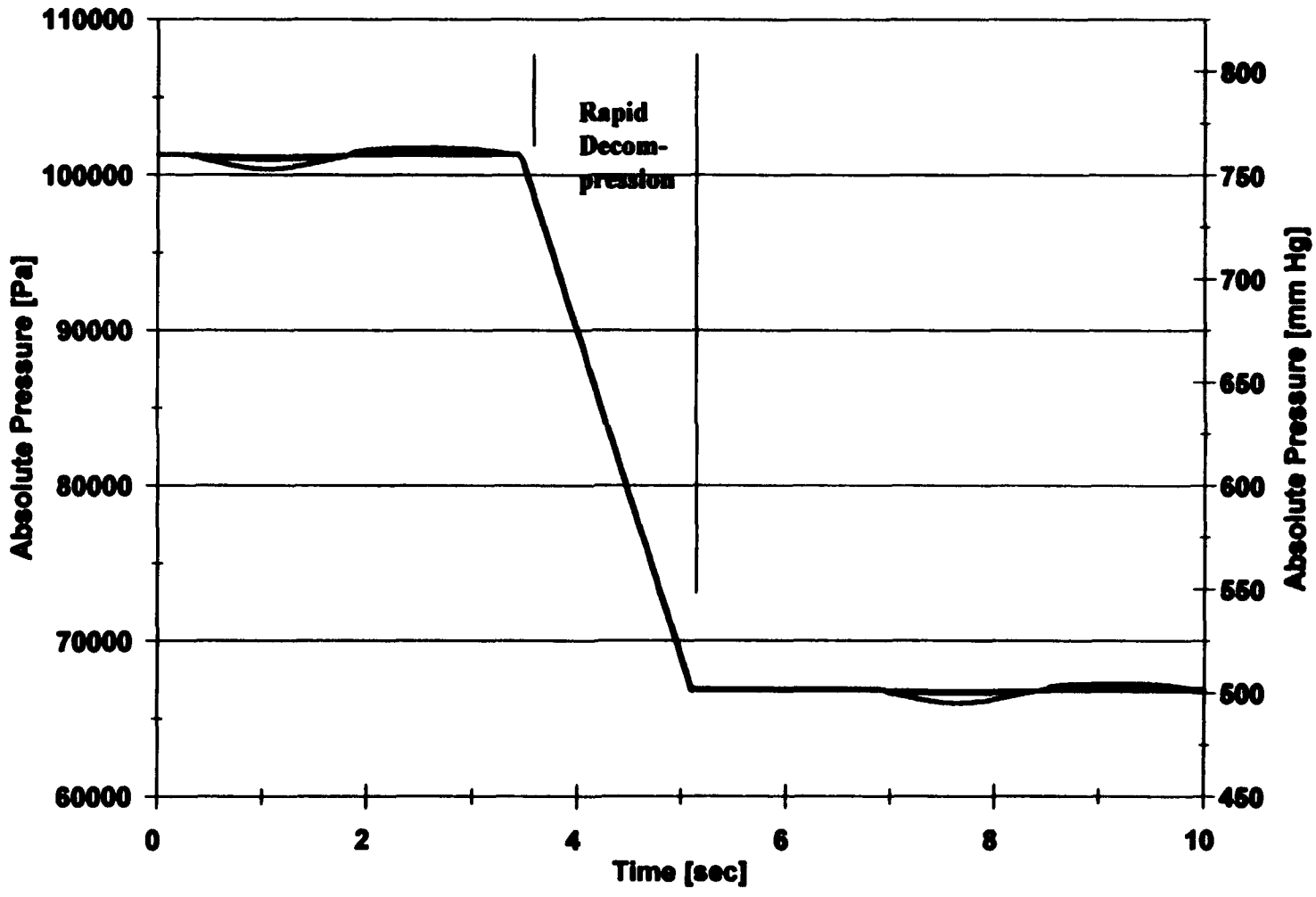

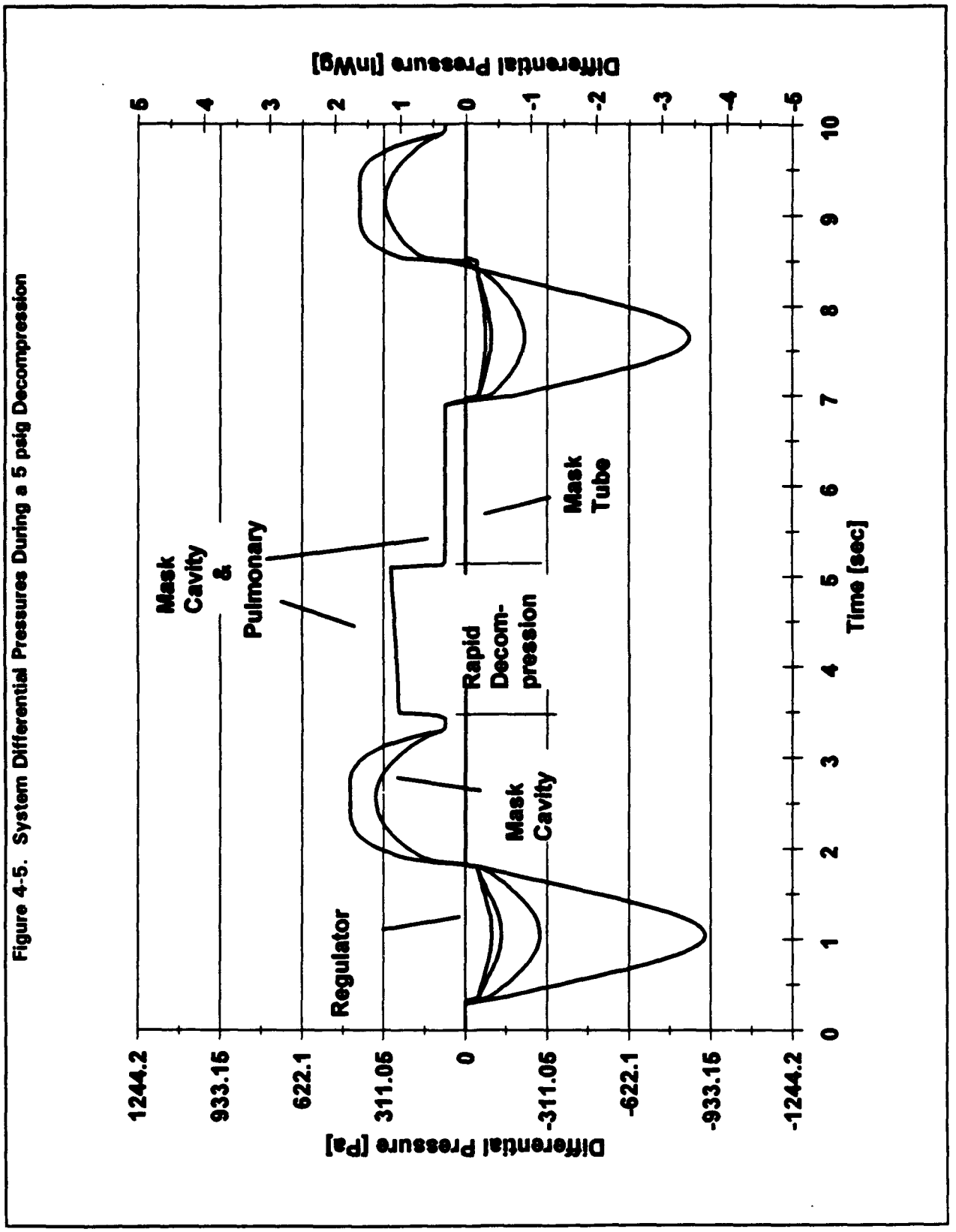

Figure 4-5. System Differential Pressures During a 5 psig Decompression

Figure 4-6. System Flows

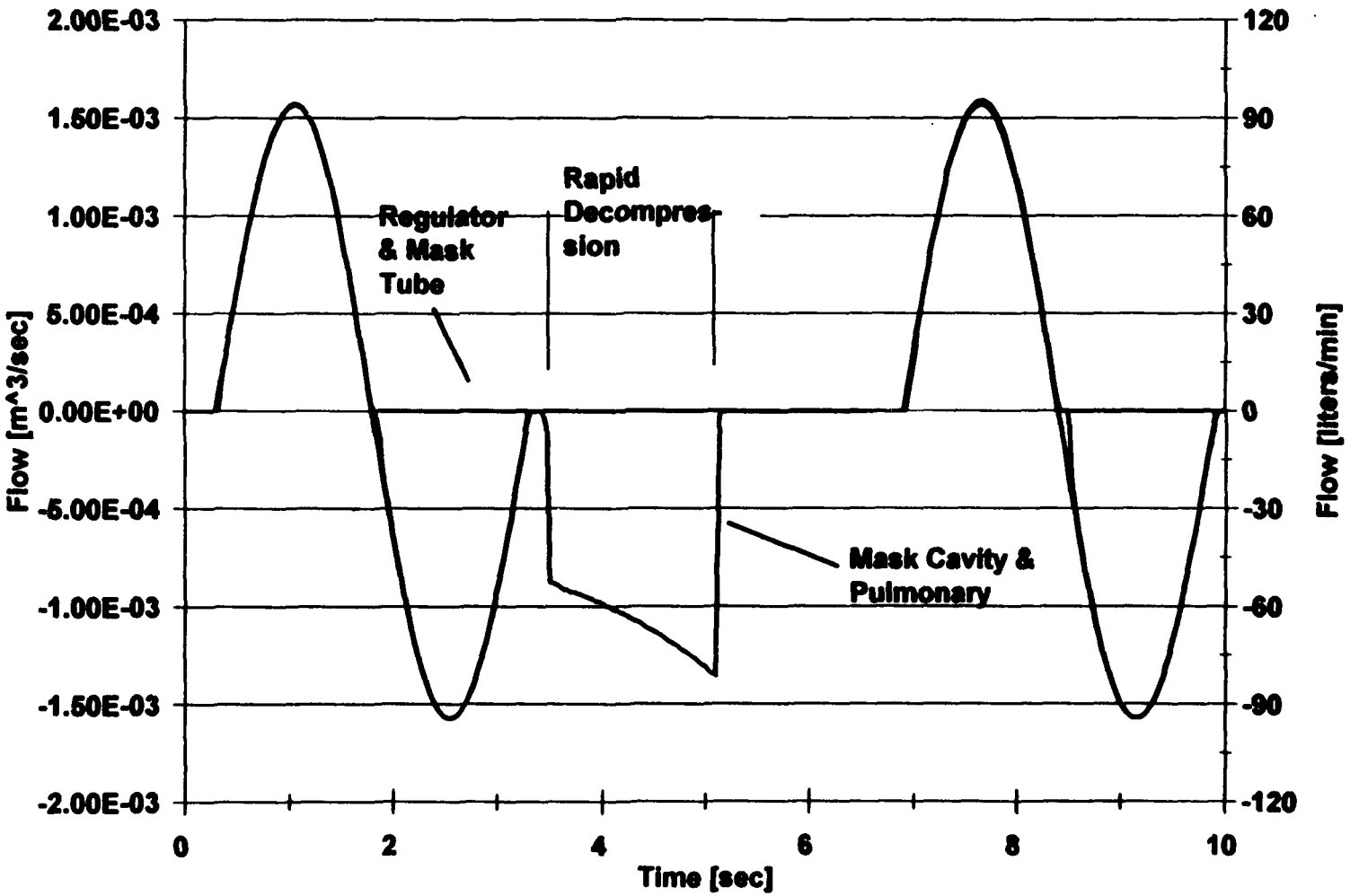

SECTION 5.0

5.0 Pulmonary Model.

5.1 Overview.

The Pulmonary Model describes the vertical ventilation pattern in the lungs and the concentration of a tracer gas throughout the lungs during a breath. Two computerized models comprise the Pulmonary Model. In these models, each lung is made up of four regions of equal mass that are located at different vertical positions. Figure 5-1 gives an overview of the inputs and outputs of the two models. The first, the Ventilation Model, determines the ventilation pattern along the vertical axis of the lung. The results of this model are input into a second model, the Convection-Diffusion Model, which calculates the concentration of a tracer gas throughout each lung during a breath. The Pulmonary Model is designed to simulate experiments. Flows measured at the mouth during a breath are read into the Ventilation Model and the output from the Convection-Diffusion Model, the exhaled gas concentration at the mouth, can be compared with the measured concentrations.

Figure 5-1. Overview of the Pulmonary Model Inputs and Outputs and the Validation Process

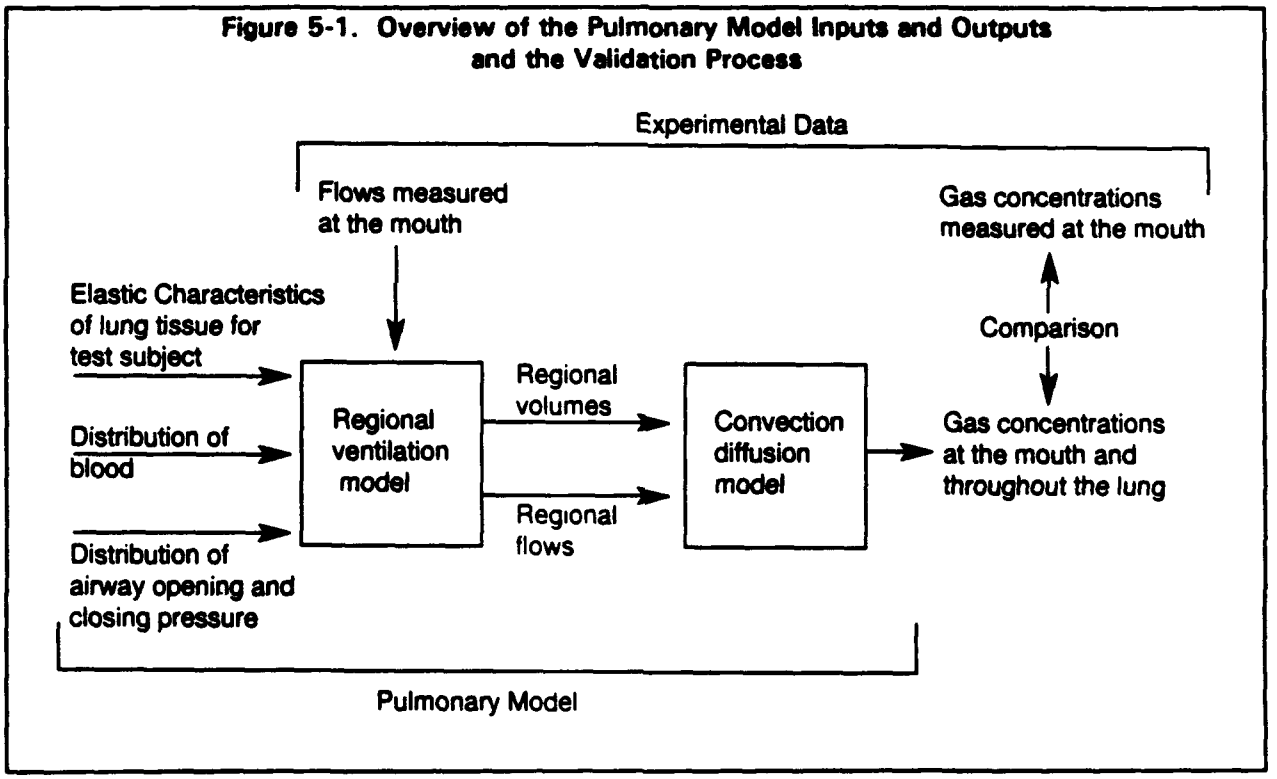

The Ventilation Model calculates that large volume and ventilation differences that are created by gravity, which have traditionally been called "interregional differences" by physiologists.[10] The interregional volume and ventilation differences are a result of the stress field in the lung tissue that supports the weight of the lung tissue and blood.[30] The Ventilation Model calculates the stress and strain of the tissue at vertical positions during slow and rapid breaths. By knowing the strain of the tissue at different lung volumes, the

regional ventilation pattern can be determined. Besides gravity, the other important parameters in the Ventilation Model are the shape of the lungs, the kinematics of the pleural boundary, the blood volume and distribution, the airway lengths and diameters, the pressure losses in the airways and the elastic characteristics of the lung parenchyma.

The Ventilation Model is made up of four regions, each positioned at a different vertical location as shown in Figure 5-2. Each region is connected to the trachea by a symmetric system of conducting airways. The position of the first three airway generations is shown in Figure 5-2. The elastic characteristics of the tissue in each region are developed through a tissue model. The gas pressures in each region are found by calculating the pressure losses in the gas as it flows through the conducting airways of that region. The regional flows for a given flow at the mouth are calculated by balancing the tissue pressures, the gas pressures in the airways and the weight of the tissue and blood in the model. The output from the Ventilation Model is the four regional volumes and the regional flows during a breath. In order to validate this model experiments in which a bolus of radioactive xenon gas was inhaled and then exhaled have been simulated.

The Convection-Diffusion Model calculates the distribution of a tracer gas along the axial pathways in the lung by solving the one-dimensional convection-diffusion equation. This model is also comprised of four regions that ventilate in parallel. The gas volume of each of the conducting airways in each region is represented physically in this model as a single trumpet shaped channel, as shown in Figure 5-3. The length of the model is the axial length down an airway, while the area of the channel is the total cross-sectional area of all the airways of a particular airway generation. The regional volumes and bulk flows in each region during a breath are calculated with the Ventilation Model. Using these flows and volumes, the one dimensional convection-diffusion equation is numerically solved in each region to determine the specific concentrations of a single tracer gas throughout the four regions during a breath. Single breath nitrogen (N_2) washout tests are simulated with the model in order to validate it.

5.2 Ventilation Model.

5.2.1 Theory.

The lung parenchyma is assumed to be isotropic and homogeneous, i.e. the tissue and gas form a continuous material. A system of symmetric conducting airways deliver gas to the alveoli in each region. Normal forces at the pleural surface are the only forces supporting the lung weight and the lung is free to slide over the pleural boundary. In order to simplify the problem, it is also assumed that the tissue does not generate a shear stress to oppose a shear strain.

Figure 5-2. The Four Regions of the Pulmonary Model. The First Three Airway Generations (Gens 1-3) and the Trachea (Gen 0) Are Shown.

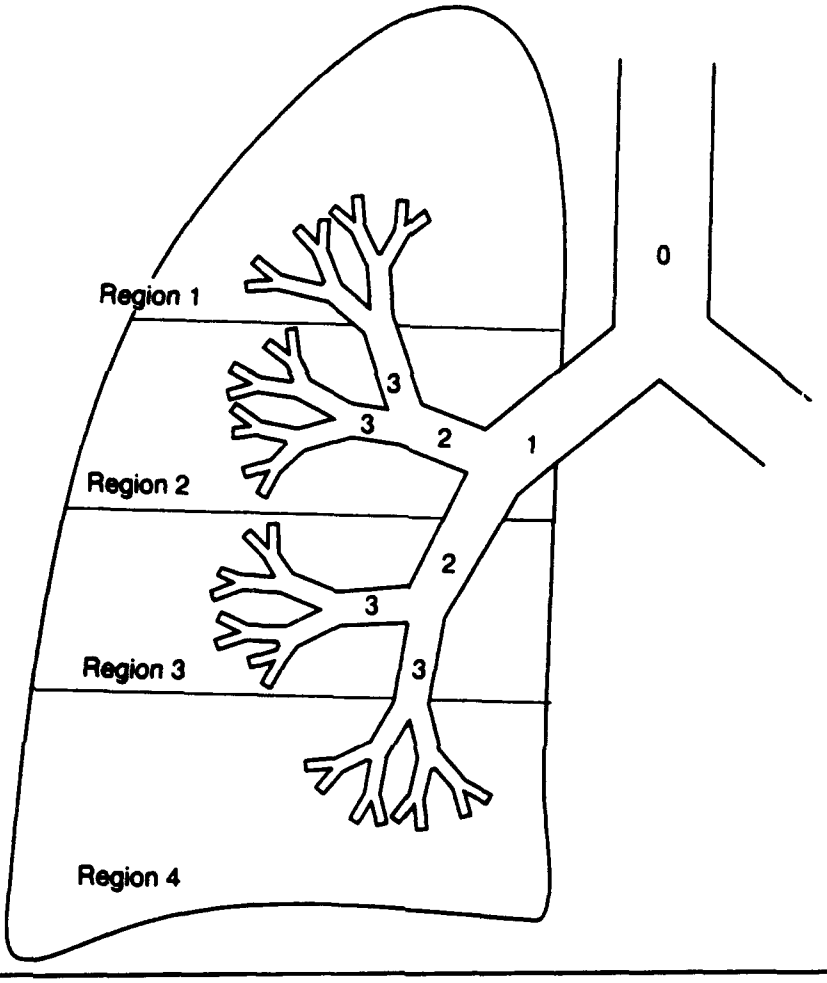

A free body diagram of a thin horizontal section of the idealized lung parenchyma with a thickness Δz is show in Figure 5-4. These distance from the lung apex to top surface is z, A is the cross sectional area of the section at z, Ppl is the pleural pressure at z, ρ is average density of the homogeneous material in the section and g is the acceleration due to gravity.

The force acting on the upper surface is A(P-Palv) and the force acting on the lower surface is

$$A(P-Palv)+\frac{d}{dz}(A(P-Palv))\Delta z \quad . \qquad [5\text{-}7]$$

Figure 5-3. The Trumpet Shaped Channel That Is Used to Represent the Airways of Each Region in the Convection-Diffusion Model

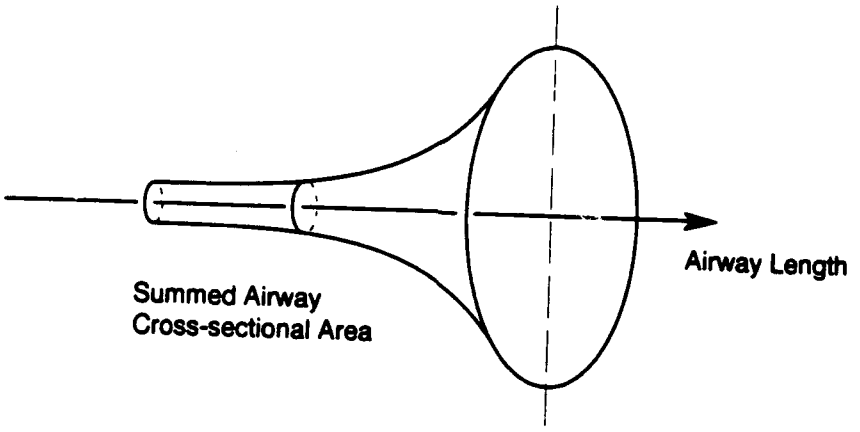

Pleural pressure acts on the outside surface and the vertical projection of this force is

$$Ppl(\frac{dA}{dz})\Delta z \ . \qquad [5\text{-}8]$$

Except at very low lung volumes, pleural pressure is negative and this force supports the lung weight. The weight of the section is $\rho g A \Delta Z$. The inertia of the tissue and the viscous losses that occur in the tissue while it is inflating or deflating are taken to be negligible. Therefore, equilibrium requires that the forces up must be equal the forces down. Equating the vertical forces in Figure 5-4 and simplifying yields the following expression

$$\frac{d}{dz}\,[A(P-Palv)]\ \Delta z + (P-Palv)\ \frac{dA}{dz}\ \Delta z + Ppl\ \frac{dA}{dz}\ \Delta z + g\rho A\Delta z = 0 \ . \qquad [5\text{-}9]$$

Static equilibrium at the pleural surface requires that $Ppl = -(P-Palv)$ and Equation 5-9 becomes

$$\frac{dP}{dz} - \frac{dPalv}{dz} = -g\rho \ . \qquad [5\text{-}10]$$

Figure 5-4. Free-Body Diagram of a Thin Horizontal Slice of Lung Tissue

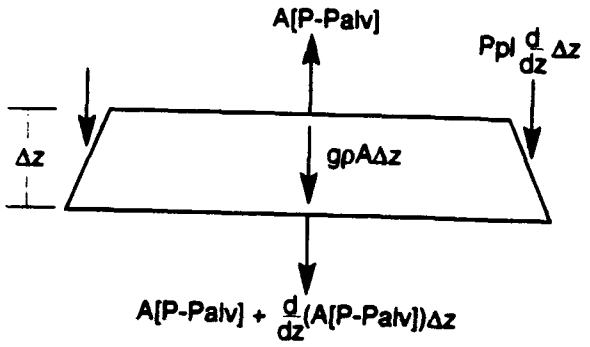

The tissue pressure gradient, dp/dz, is a function of the vertical gradient in the alveolar pressure as well as the tissue density. If Equation 5-10 is integrated between two vertical positions z_i and z_j, then

$$P_i - P_j = \int_{z_i}^{z_j} \rho dz + (Palv_i - Palv_j) \ , \qquad [5\text{-}11]$$

where the integral term represents the pressure difference created by the weight of the tissue and blood and the subscript indicates the vertical location.

The difference in the alveolar pressures between two vertical regions is obtained by calculating the gas pressures in the bronchi that connect the two regions. Any two regions in the lung have airway that meet at some bronchus which is called the meeting bronchus. As shown in Figure 5-5, the alveolar pressure of each region minus the pressure difference, ΔPaw, between the alveolar gas and the gas pressure at the meeting bronchus equals the pressure at the distal end of the meeting bronchus

$$Palv_i - \Delta Paw_i = Palv_j - \Delta Paw_j \ . \qquad [5\text{-}12]$$

In Figure 5-5 the Pbr is the bronchial pressure and the n subscript is the generation number. The pressure change along the airway, ΔPaw, equals the sum of the pressure losses across each bronchus δP in the pathway between the alveoli, which start at generation 17, and the meeting bronchus

Figure 5-5. Pressure Change Between the Meeting Bronchus and the Alveoli (ΔPaw) of Two Lung Regions

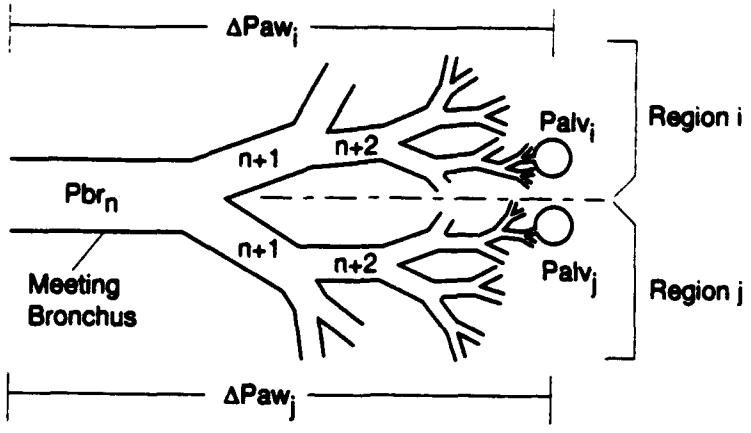

$$\Delta Paw_i = \sum_{n=16}^{\text{meeting bronchus}} \delta Pbr_n \qquad [5\text{-}13]$$

where the pressure change across each bronchus equals the pressure at the distal end of the bronchus minus the pressure at the proximal end. The pressure change in each bronchus is due to viscous losses (δPv) and convective pressure changes (δPc) as the gas passes from one generation of airway to the next,[31]

$$\delta Pbr = \delta Pv + \delta Pc \ . \qquad [5\text{-}14]$$

When Equation 5-12 is substituted into Equation 5-11,

$$P_i - P_j = g \int_{z_i}^{z_j} \rho dz + (\Delta Paw_i - \Delta Paw_j) \ . \qquad [5\text{-}15]$$

The regional volumes and flows in the Ventilation Model are calculated by satisfying Equation 5-15.

5.2.2 The Lung Model.

As shown in Figure 5-2, each lung is represented as four regions that ventilate in parallel. Each region has the same tissue mass. The pressures throughout a region are constant except in the neighborhood of the larger bronchi where the local tissue pressure depends on the relative expansion of the bronchi compared to the expansion of the tissue in the region. The alveolar gas volume in each region is connected to the trachea by a homogeneous system of conducting airways. In a homogeneous airway system, each pathway from the trachea to the alveolated airways is identical. The gas flow through each pathway within a region is taken to be the same, therefore, the pressure change ΔPaw is the same for all airways in a region and the alveolar pressure is the same throughout a region. Weibel's Symmetric Lung Model A[30] is used to obtain the lengths and diameters of each of the airway generations in the Ventilation Model. In Weibel's Symmetric Lung Model A, the lung is composed of a symmetric airway system of 23 generations. Each airway division distal from the trachea is labelled as a generation. Generation 1 is the two airways that connect the right and left lung to the trachea and generation 23 is the deepest airway. Alveoli start at generation 17. Table 5-1 lists the lengths and diameters of the airways in this model.

Figure 5-2 shows the lung model along with the first three airway generations. Generations 4-16 are all located in the region where the third generation ends. The bronchial pressures in generations 1-16 are calculated in the Ventilation Model. The gas velocities in the higher generations are too low to produce significant pressure changes. All four regions of the model meet at the first generation, and so generation 1 is the meeting bronchus in Equation 5-15.

5.2.3 Parenchymal Elastic Recoil Characteristics.

A model of the lung tissue was developed as part of the Ventilation Model in order to take into account the elastic characteristics of the tissue, the shape of the lung, the blood volume in the lung, the general elastic characteristics of the tissue and the effect of airway closure and opening. This model determines the tissue elastic characteristics of a test subject from data on their residual volume (RV), total lung capacity (TLC) and their measured lung pressure-volume characteristics.

The basic mechanical unit of the tissue model consists of a single terminal bronchus (generation 17) which services a respiratory unit (generations 18-23). The mechanical unit represents the gas exchanging portion of the lungs which comprises more than 90% of the gas volume of the lung. All respiratory units in the tissue model are identical. The respiratory unit can remain patent until zero gas volume, but the terminal bronchus, which is the sight of airway closure in the lungs,[32] acts as a valve which is either fully open or closed. A pressure-fractional volume curve for the respiratory unit (P-FVru) could be constructed by expanding the unit from the completely collapsed state, zero gas volume, to its maximum volume and then deflating the unit back to zero volume. The fractional volume (FV) is the volume of a lung unit normalized with respect to its maximal volume. The gas

Table 5-1. Weibel's Symmetric Lung Model A,
Total Volume of Lung Model (Vm) is 4820 cc.

Airway Generation	Number of Airways per Generation (NPG)	Generation Length *l* (cm)	Generation Diameter *d* (cm)	Alveolar Volume per Generation Valv (cc)
1	2	4.76	1.22	
2	4	1.90	0.83	
3	8	0.76	0.56	
4	16	1.27	0.45	
5	32	1.07	0.35	
6	64	0.90	0.28	
7	128	0.76	0.23	
8	256	0.64	0.186	
9	512	0.54	0.154	
10	1024	0.46	0.130	
11	2048	0.39	0.109	
12	4096	0.33	0.095	
13	8192	0.27	0.082	
14	16384	0.23	0.074	
15	32768	0.20	0.066	
16	65536	0.165	0.060	
17	131072	0.141	0.054	6.4
18	262144	0.117	0.050	22.2
19	524288	0.099	0.047	63.2
20	1048576	0.083	0.045	222.2
21	2097152	0.070	0.043	444.5
22	4194304	0.059	0.041	892.2
23	8388608	0.050	0.041	1523.0

pressure measured at a volume when the lung unit is sealed reflects the tension in the tissue and is called the elastic recoil pressure (P) or simply the unit pressure. The P-FVru curves used in the tissue model are obtained by extrapolating the upper half of a lung pressure-volume curve (P-FVlung) to zero gas volume. At a fractional gas volume greater than 0.50 all of the airways are presumed open and the lung pressure-fractional volume curve and tissue fractional volume curve should be similar. A cubic curve is used to describe the upper half of the lung pressure-fractional volume curve and a straight line is used to describe the lower half, as given in the following equation.

$$FVmu(P) = \alpha(P-P_{0.0}) - \beta(P-P_{0.5})^3$$
$$\beta = 0 \text{ for } 0 \le FVmu \le 0.5$$
$$\beta = 16\ \alpha\ \frac{3}{27} \text{ for } 0.5 < FVmu \le 1.0 \qquad [5\text{-}16]$$

The value of α for a subject is determined from the linear part of his P-FVlung curve, which is between approximately 20% and 80% of the vital capacity (VC). The value of $P_{0.5}$ equals the transpulmonary pressure at FVlung = 0.5 during inhalation and exhalation. The dashed line in Figure 5-6 shows the P-FVru relation for a subject with $P_{0.5}$ = 5 cmH_20 during exhalation, α = 0.05 cmH_20 and a hysteresis of 4 cmH_20 during a VC breath. Both the inhalation and exhalation curves are taken to have the same shape, only they are separated by the hysteresis.

The state of each terminal bronchus, whether it is open or closed, depends on the transmural (Ptm) that acts on it. The transmural pressure is defined as the intrabronchial gas pressure (Pbr) minus extrabronchial pressure (Px), the pressure acting on the outside wall. Since the terminal bronchi are deeply embedded in the tissue, the extrabronchial pressure equals pleural pressure under the no flow condition, so the transmural pressure acting on the terminal bronchi equals pleural pressure under no flow conditions.

The transmural pressure at which a terminal bronchus closes is called the critical closing pressure (Pcc). The amount of gas trapped and the minimum gas volume of each respiratory unit is determined by the critical closing pressure of its terminal bronchus. Once closed each terminal bronchus requires a significantly higher transmural pressure before reopening. The transmural pressure at which the terminal bronchus reopens is called the critical opening pressure (Pco). Unfortunately, there is little data available on the distribution of the critical pressures so it is taken to have a normal distribution. The mean critical opening and closing pressure of the probability density function are $\overline{Pcc}$ and $\overline{Pco}$ and the standard deviations of the distributions are σcc and σco. The sequence of the terminal bronchi opening is taken to be the opposite of the closing sequence, i.e. the first airways to close are the last to open. The maximum range of the critical pressures has been estimated to be 4.0 cmH_20[33] and the

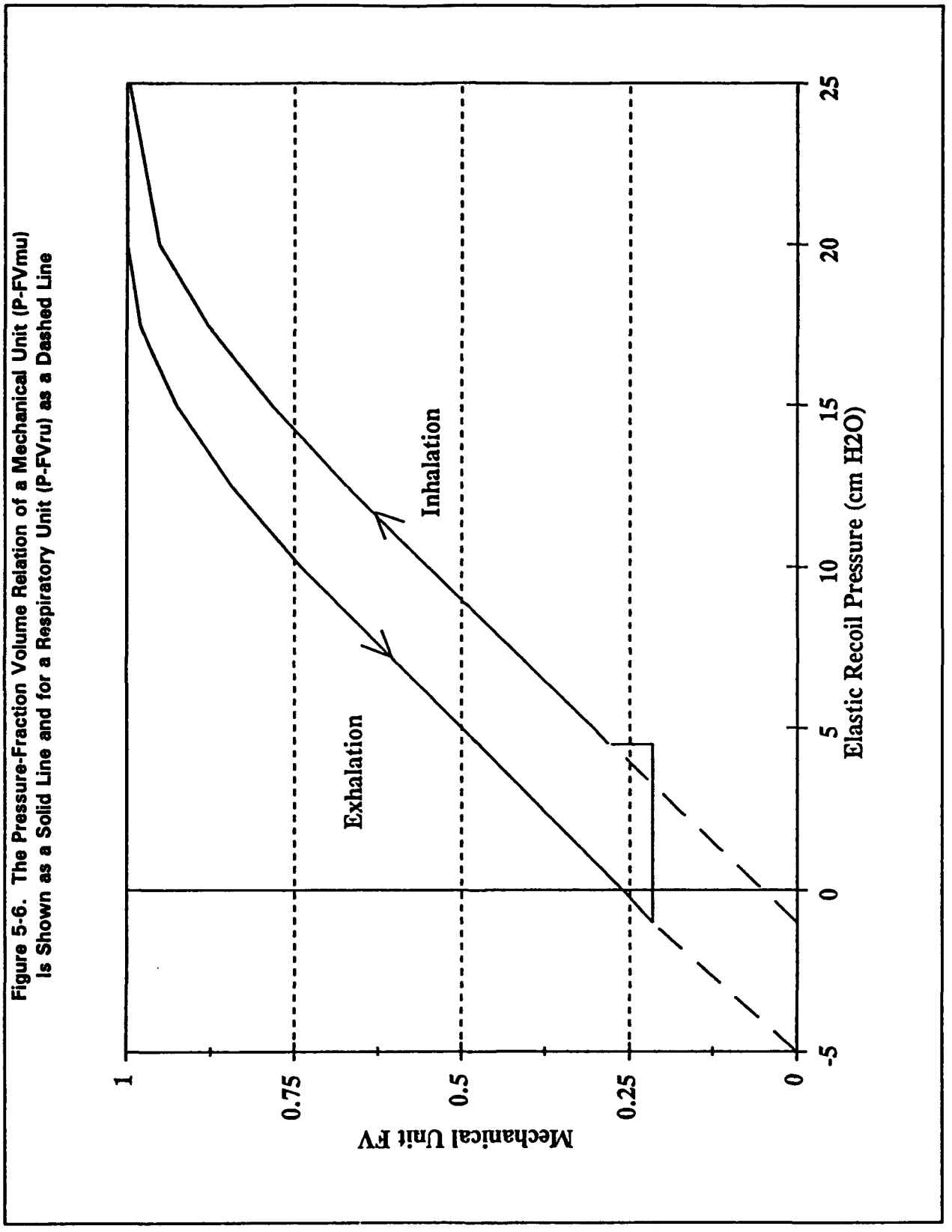

Figure 5-6. The Pressure-Fraction Volume Relation of a Mechanical Unit (P-FVmu) Is Shown as a Solid Line and for a Respiratory Unit (P-FVru) as a Dashed Line

standard deviations of the critical pressures are $\sigma cc = 0.5$ and $\sigma co = 0.8$. Figure 5-7 shows examples of the probability density functions for the critical opening and closing pressures.

Figure 5-7. Example of Probability Density Function for Critical Closing/Opening Pressures of Terminal Bronchi Used in Tissue Model
Pcc = -0.8 cmH_2O, Pco = 4.2 cmH_2O

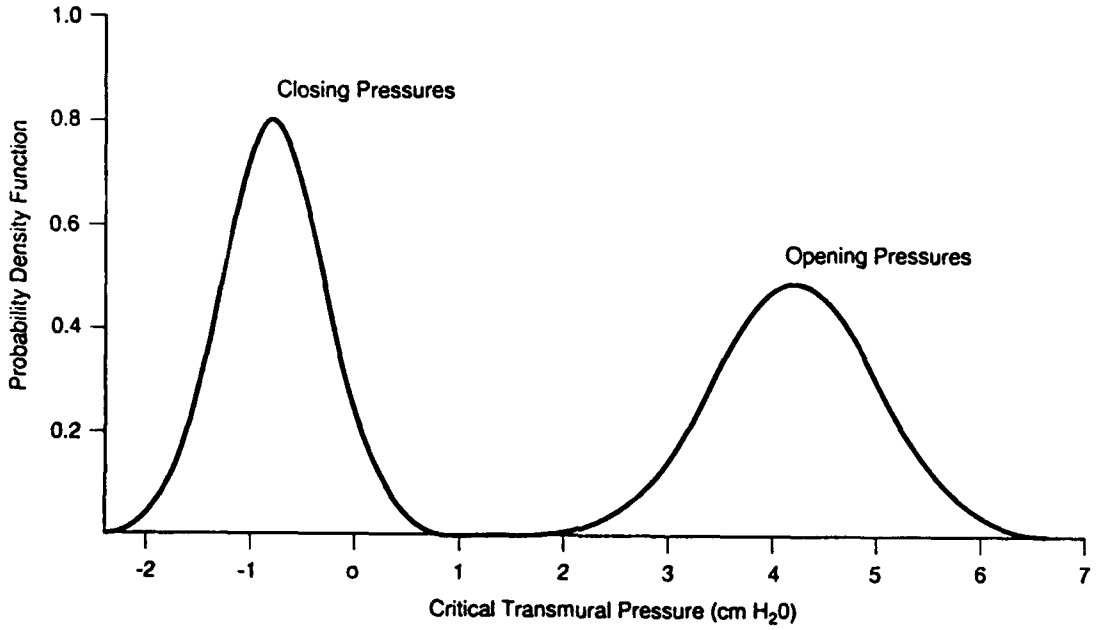

The pressure-fractional volume relation of the mechanical unit (P-FVmu) represents the elastic characteristics of the respiratory unit and its terminal bronchus. The P-FVmu curve is identical to the P-FVru curve as long as the terminal bronchus remains open. Once the terminal bronchus closes, the mechanical unit is incompressible and any further lowering of the tissue pressure causes no decrease in gas volume. The P-FVmu of a mechanical unit during a vital capacity breath is shown in Figure 5-6 as a solid line. The terminal bronchus of this mechanical unit has a Pcc = 0.0 cmH_2O and Pco = 5 cmH_2O. During exhalation, once the terminal bronchus closes, the mechanical unit is incompressible and the fractional volume remains at 0.2. When the tissue pressure is increased to 5 cmH_2O, the terminal bronchus reopens and the mechanical unit rapidly expands to its new equilibrium state on the P-FVru curve.

The fractional gas volume of the tissue at a pressure P equals the sum of the fractional gas volumes of all the mechanical units that comprise the tissue. The tissue pressure-fractional volume (P-FVtis) relations are obtained by accounting for the closing and subsequent opening of the terminal bronchi in all the mechanical units of the tissue. The P-FVtis curve that results when the P-FVru curve in Figure 5-6 is combined with the opening and closing distribution in Figure 5-7 is shown in Figure 5-8. The code used to calculate the P-FVtis curve is given in Appendix C-1.

The total tissue mass of the lungs is taken to be a function of a subject's TLC. At TLC all regions of the lung are fully expanded and have the same density of 0.12 $gm \cdot cm^{-3}$ per cc. RV varies from subject to subject and in the same subject. For each subject the ratio of RV divided by TLC and the tissue minimum fractional volume ($FVtis_{min}$) are important parameters in calculating the lung pressure-fractional volume relation at low lung volumes because these parameters determine the fraction of the respiratory units that are closed at low lung volumes. In order to quantify the relation between RV/TLC and $FVtis_{min}$, a new variable is introduced, the difference between the minimal fractional volume of the lung and the tissue,

$$\psi = \left(\frac{RV}{TLC}\right) - FVtis_{min} \qquad [5\text{-}17]$$

The graphical meaning of ψ is shown in Figure 5-8, where the P-FVtis and the calculated lung Pressure-Frictional Volume (P-FVlung) curve for a subject are shown. For this subject, RV/TLC = 0.26 and $FVtis_{min}$ = 0.21, making ψ = 0.05. If all of the lung tissue at RV is not at the minimal fractional volume then $\psi > 0$, which is the case for most young, healthy subjects. If all of the lung tissue is at the minimal fractional volume then ψ = 0. Thus ψ can only be equal to or greater than zero.

There are no experimental estimates of ψ, but measurements of the fraction of airways closed at RV as a function of vertical position have been made.[33] By choosing ψ equal to 0.05, the fraction of airways closed along the vertical axis of the lung model was similar to that measured in these experiments.

The P-FVlung relation and the degree of airway closure are determined by creating a lung with a physical geometry like the human lung, a ellipsoidal shape, and solving Equation 5-10 with the alveolar pressure gradient set equal to zero,

$$\frac{dP}{dz} = -g\rho \qquad [5\text{-}18]$$

the hydrostatic pressure equation. By filling the ellipsoidal shaped lung model with the imaginary tissue and solving the hydrostatic pressure equation the P-FVlung can be

Figure 5-8. The Relation Between ψ and the P-FVtis and P-FVlung Curves. P-FVtis Is Shown as a Dashed Line and P-FVlung Is Shown as a Solid Line.

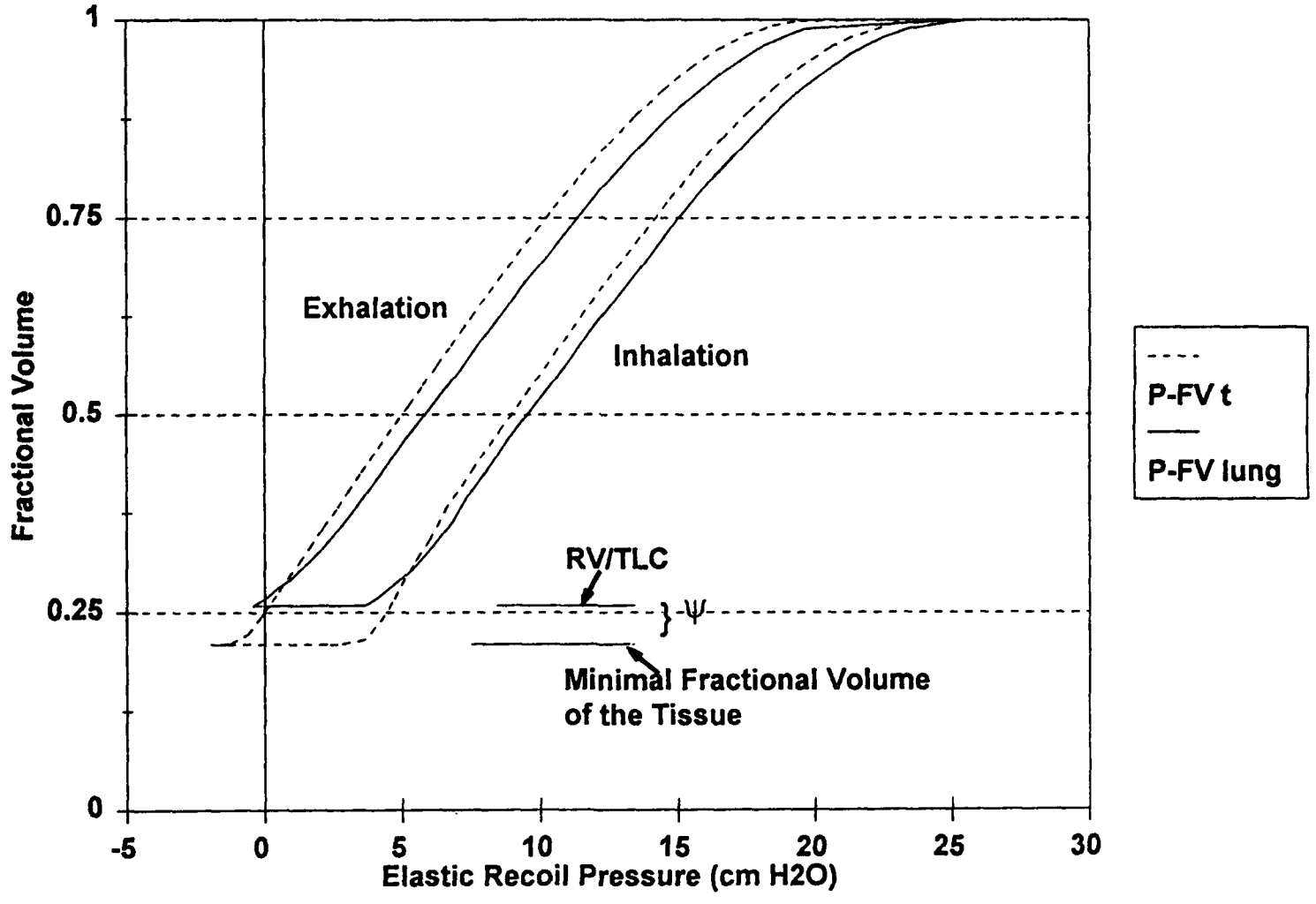

calculated. The P-FVlung relationships are obtained by dividing the ellipsoidal shaped model into fifty thin sections and numerically solving the hydrostatic pressure equation at the boundary of each slice. The lung model then performs a VC inhalation and exhalation, while the elastic recoil pressure is measured at a fixed vertical position that is similar to the position of an esophageal balloon. In doing this calculation the weight of the blood is also included in the density term. The code for calculating the P-FVlung relation is given in Appendix C-2.

5.2.4 Blood Volume Distribution

The blood volume and distribution affects the tissue pressure since supporting stresses in the tissue, the dp/dz term in Equations 5-10 and 5-15, must support the weight of the blood as well as the tissue weight. Information on the volume distribution of the blood in the pulmonary capillaries is difficult to obtain, and to the best of our knowledge, no data is available on humans, although there have been estimates[30] of total blood volume ranging from approximately 100 cm^3 to approximately 200 cm^3. In order to calculate the blood volume distribution along the vertical axis, the pulmonary capillaries are viewed as sheets that surround the alveoli.[34] The sheet area per gram of tissue is taken as a constant throughout the lung and is estimated to be 100 square centimeters per gram of tissue. The height of the capillaries (h) is calculated using experimental results.[35,36] In these studies it was found that the capillary height in cats is a linear function of the capillary transmural pressure, the pressure differences between the capillary pressure (Pcap), and the alveolar gas pressure,

$$h = h_o + h'(Pcap - Palv) \qquad [5\text{-}19]$$

where

$$h_o = 4.3 \times 10^{-4} cm \qquad [5\text{-}20]$$

and

$$h' = 2.2 \times 10^{-5} cm\ H_2O\ . \qquad [5\text{-}21]$$

This relationship holds for Pcap greater than Palv, but for negative transmural pressures the capillary is collapsed and h = 0. The capillary blood pressure is the sum of the arterial pressure generated by the heart and the hydrostatic pressure that results in the change in vertical position as the blood moves from the heart through the lungs. Figure 5-9 shows the vertical distribution in one of the lungs of the tissue model at 60% VC. The model predicts

that the blood volume will increase as lung volume increases, an increase caused by the downward movement of the base of the lung relative to the heart.

Figure 5-9. The Summed Blood Volume Moving From the Lung Apex to the Base in a Single Lung. Total Pulmonary Blood Volume Would Be Twice This Amount.

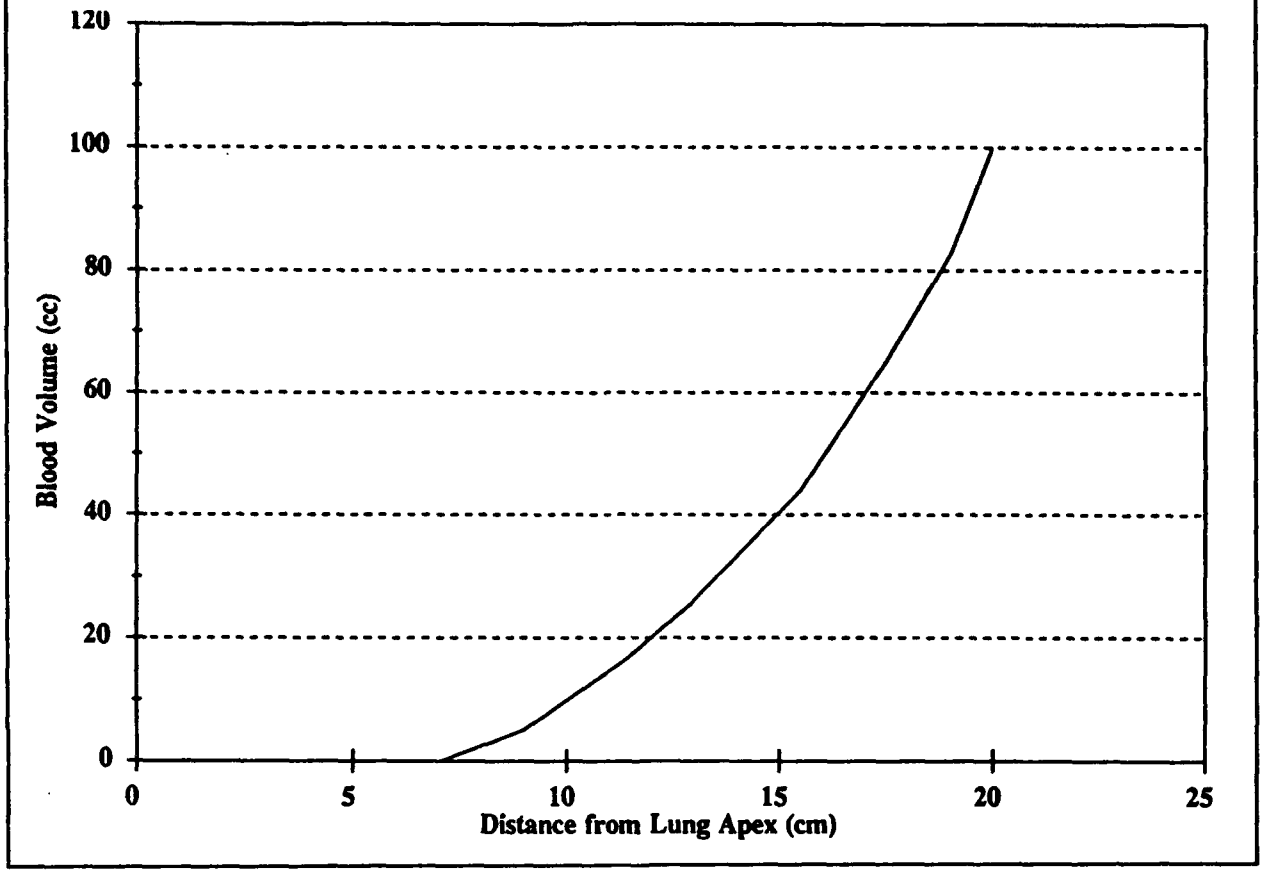

The tissue model is also used to obtain the Pressure Fractional Volume relations for each of the regions in the Ventilation Model (P-FVreg). These are obtained by dividing the fifty horizontal sections of the tissue model into four regions of equal mass. The center of gravity (CG) of each of these four regions is determined and the tissue model is taken through a VC inhalation and exhalation while the elastic recoil pressure at the regional CG's and the gas volume of the region are recorded. The other variable measured is the difference in the elastic recoil pressure between the regional CG's, which takes into account the weight of the tissue and blood between the regional CG's. The P-FVreg curves represent the elastic characteristics of each of the four regions in the Ventilation Model.

5.2.5 Transmural Pressures Acting on the Bronchi

The bronchi in the Ventilation Model are treated as compliant tubes whose diameters are a function of the transmural pressure acting on their walls. The transmural pressure (Ptm)

equals the gas pressure inside the bronchus (Pbr) minus the extrabronchial pressure (Px), the pressure acting on the outside wall of the bronchus,

$$Ptm = Pbr - Px \ . \qquad [5\text{-}22]$$

The tissue pressure throughout each region of the model is equal to P except in the neighborhood of the larger bronchi. The extrabronchial pressure is the sum of the local tissue pressure and the alveolar pressure. Px depends on how the bronchus is expanded relative to the tissue in the surrounding lung region since there is a mechanical interdependence between the bronchus and the tissue that surrounds it.[37,38] If the bronchus expands uniformly with the surrounding region, then the extrabronchial pressure equals the pleural pressure. In this case, the tissue around the bronchus expands as if the space occupied by the bronchus was filled with tissue.

When a bronchus does not expand uniformly with the surrounding tissue, the local tissue pressure does not equal the regional tissue pressure and Px no longer equals pleural pressure. For example, during a rapid exhalation, the bronchi deflate faster than the surrounding tissue because they can be exposed to large negative Ptm's. When this happens, Px becomes greater than the pleural pressure because of the mechanical interdependence and this increase in Px aids in keeping the bronchi from collapsing. The effect of bronchial and tissue interdependence in the Ventilation Model is assumed to be important during exhalation, it is taken to be insignificant during inhalation. The magnitude of the mechanical interdependence has been estimated using the interdependence parameter that was introduced to explain some experimental data.[38] The transmural pressure is calculated by solving the following equation,

$$Ptm = P - (\frac{1}{K})\Delta Paw \qquad [5\text{-}23]$$

where P is the regional elastic recoil pressure, ΔPaw is the total pressure change between the alveoli and that airway, and K is the interdependence parameter which ranges from one to approximately three.

The elastic properties of the bronchi and the tissue have been shown to be similar.[39] Therefore, the bronchial diameters and lengths are treated as a function of the gas volume of the lung V and varied with the cube root of the fractional gas volume of the lung

$$\frac{l}{l_{max}} = \frac{d}{d_{max}} = (\frac{V}{TLC})^{\frac{1}{3}} \qquad [5\text{-}24]$$

where l is the length and d is the diameter of an airway generation and l_{max} and d_{max} are the maximum airway lengths for a generation at TLC. Equation 5-24 is used to solve for the relative lengths and diameters of the bronchi.

During exhalation the bronchi are exposed to negative transmural pressures. Unfortunately, there are limited data on the diameters changes of the bronchi under negative transmural pressures. During exhalation the conducting airway system and latex tubes both exhibit flow limitation, that is the flow approaches an asymptote (for a constant lung volume) as the applied pressure is increased. The relation of the airway diameter d to a negative transmural pressure is described by the modified tube law,[40]

$$d = d_o(1 - \frac{Ptm}{\epsilon}) \qquad [5\text{-}25]$$

where d_o is the airway diameter of a generation at Ptm = 0 and the coefficient ϵ is proportional to the bending stiffness of the bronchial wall at Ptm = 0.

5.2.6 Solution Procedure.

The regional flows are calculated for a given flow at the mouth Qm at a given lung volume. The calculation is made simultaneously solving Equation 5-15 and equation of conservation of mass,

$$Qm = Q_1 + Q_2 + Q_3 + Q_4 \qquad [5\text{-}26]$$

where the Q_1, Q_2, Q_3, and Q_4 are the regional flows. The calculation of the regional flows is done numerically. The breath is divided into small time increments of size Δt and the regional flows are calculated at the end of each time increment by determining the regional flows that satisfy Equation 5-15 and the conservation of mass, Equation 5-26. The code for the Ventilation Model is given in Appendix C-3.

5.2.7 Model Results and Validation.

Figure 5-10 shows the volumes of the four regions of the Ventilation Model during a slow VC inhalation by a subject with a RV of 2 liters and a TLC of 7.5 liters. The tissue P-FVtis and lung P-FVlung relation for this subject are shown in Figure 5-8. The distribution of opening and closing pressures for this subject are shown in Figure 5-7.

Figure 5-10 provides a good overview of the interregional ventilation differences during a slow breath. The VC for this subject was 5.6 liters. Most of the gas inhaled near RV enters the apical regions, Regions 1 and 2, and the volume curves for these two regions have the steepest slope. Region 4 undergoes the smallest expansion during the inhalation of the first

Figure 5-10. Regional Gas Volumes vs. % VC During a VC Breath.
The Positions of the Four Regions are Shown in Figure 5-2

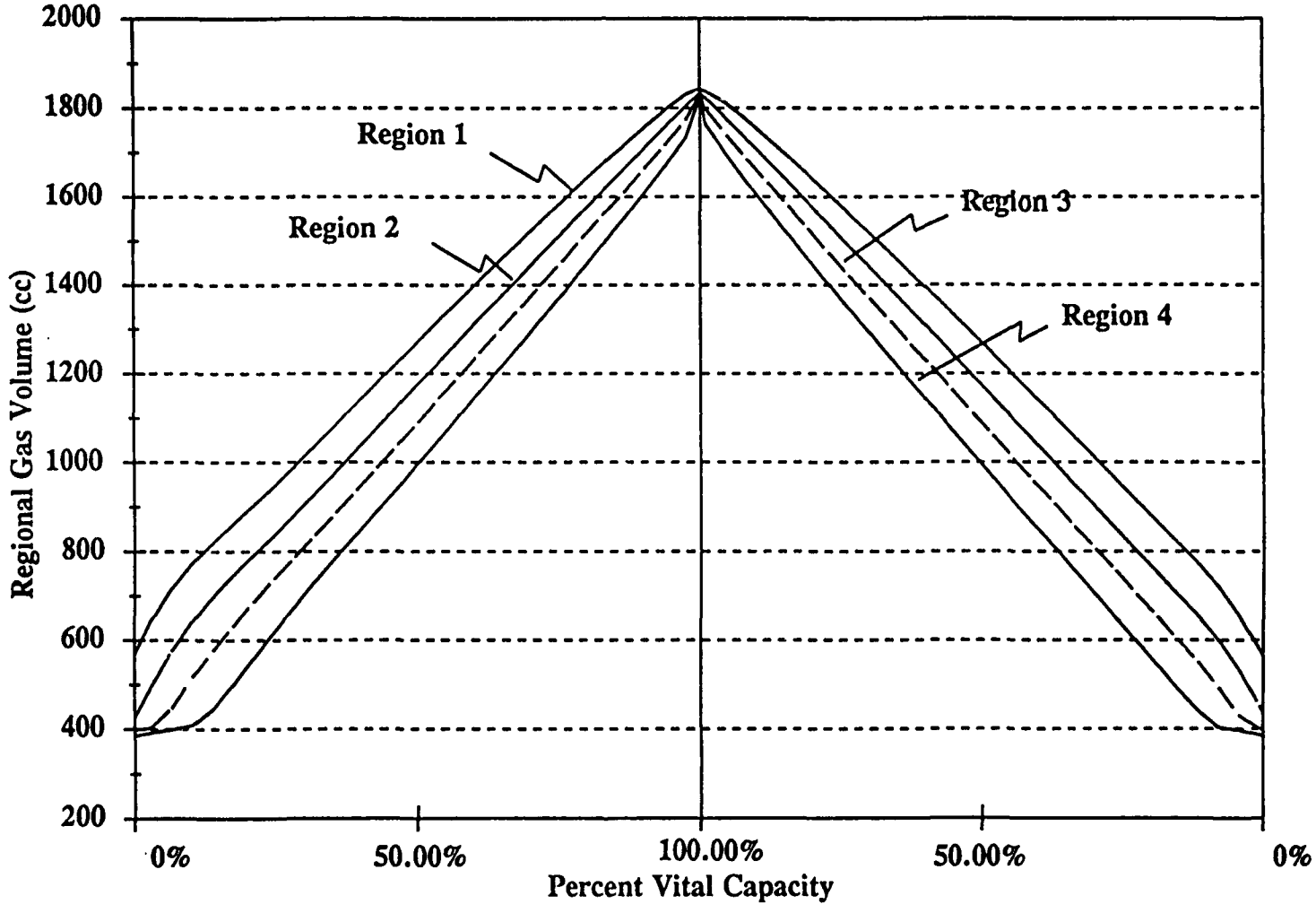

liter of gas because it contains such a large fraction of closed terminal bronchi. Once all the terminal bronchi open, the basilar regions become more compliant and take in a larger fraction of the inhaled gas, as indicated by the steeper slope of the regional volume curves for Regions 3 and 4 after 1.5 liters of gas have been inhaled. This causes the regional volume differences to decrease as lung volume increases. At TLC, the four regions contain almost the same amounts of gas.

The emptying of the four regions is also sequential, the slope of the volume curve for Regions 1 and 2 becomes progressively steeper as the gas volume decreases, the two apical regions contribute more gas to the expiate as lung volume decreases. Initially the basilar regions contribute the largest fraction of gas and their gas volumes decrease the fastest. As lung volume approaches RV, the terminal bronchi in the basilar regions begin to close, reducing the flow from these regions and the regional volume curve for Region 4 becomes flatter. At the end of exhalation, almost all of the decrease in total gas volume occurs in the upper two regions because of the large fraction of closed terminal bronchi in the basilar regions. This plot of the volume change of regions at different vertical positions agrees with experimentally measured curves of regional volume changes.[41]

The Ventilation Model has been used to calculate both the inhaled distribution and the subsequent washout of radioactive xenon (Xe) gas.[42,43] In these experiments, a subject inhales a bolus of radioactive Xe gas at different lung volumes and at different inhalation flow rates. At the end of inhalation, the subject performs a breath hold and the vertical concentration of Xe gas in the lungs is measured. During the subsequent exhalation, the Xe concentration at the mouth is measured.

In order to perform an accurate simulation of the Xe washin experiments, the transport of the bolus through the upper airways, the mouth, the pharynx and trachea is analytically modeled. This is done by representing the upper airways as a pipe with a cross-sectional area of 2.5 cm^2 and a length of 25 cm. A Xe bolus of 5 cm^2 is placed at the pipe entrance and convected down the pipe with a uniform velocity. The mixing in the pipe is calculated by using an effective dispersion coefficient. The bolus is mixed with air as it moves through the upper airways and by the time it reaches the end of the pipe, approximately 125 cm^2 of gas contains radiation in the slow inhalation. The end inhalation Xe concentrations calculated with the Ventilation Model reflect how the model expands during the inhalation of this 125 cm^2 of gas. During the subsequent exhalation, the washout of the Xe at the mouth is recorded as a function of the exhaled volume. If there are Xe concentration differences in the lung at the end of inhalation, the Xe concentration at the mouth reflects the emptying pattern of the different lung regions during exhalation.

The results of the inhalation simulations are shown in Figures 5-11 and 5-12 for slow inhalations and fast inhalations. The results are expressed as Xe concentration versus z, the vertical height of the lung. The concentrations are shown for an Xe bolus inhaled at RV in Figure 5-11 and at 55% VC in Figure 5-12. The Xe that enters each region is assumed to be completely mixed in the alveolar gas of the region. The Xe concentration curves for each

Figure 5-11. Xe Concentration at the End of Inhalation (TLC) for a Xe Bolus Inhaled Slowly and Rapidly at RV.

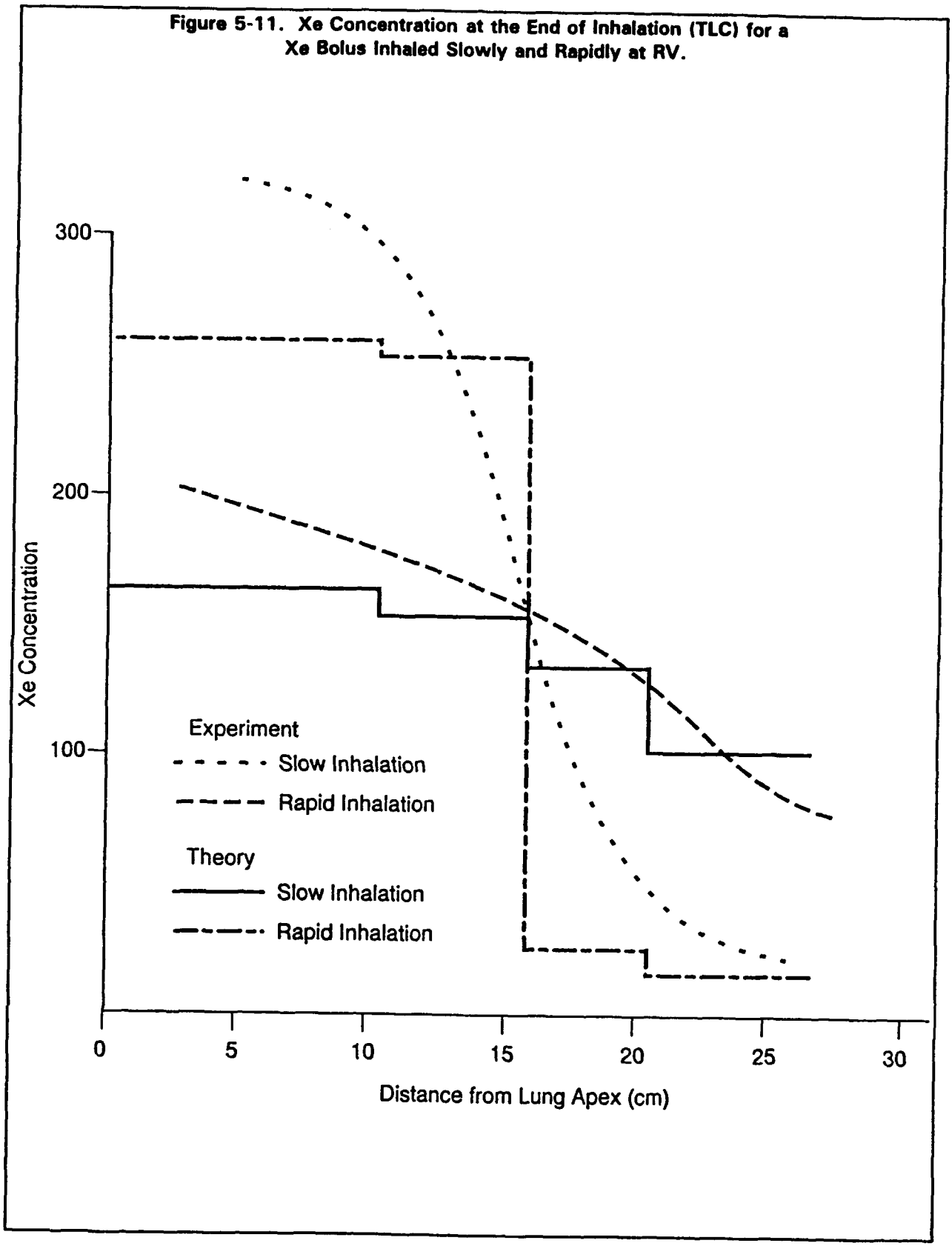

region of the model are horizontal lines when plotted against z, thus the step shaped appearance of the curves in Figures 5-11 and 5-12.

The agreement between the calculated and measured end inhalation Xe concentrations is good. Both the measured and calculated results show that as the inhalation flow rate increases, the distribution of the Xe along the vertical axis becomes more uniform. In the Ventilation Model, the fraction of the flow going to the upper half near RV decreases as the inhalation flow rate increases. At 55% VC the measured and calculated end inhalation concentrations are also similar. Both the measured and calculated Xe concentrations show that as the flow rate is increased, the distribution of the inhaled bolus in the lung becomes more uniform. The good agreement between the calculated and measured results indicates that the Ventilation Model accurately describes the filling pattern of the lung near RV and 55% VC for different flow rates.

The measured single breath washout curve for a rapid exhalation starting at TLC were not available in the study that investigated the inhalation distribution of the Xe bolus. A similar study did publish Xe single breath washout curves for different exhalation flows, but no data was given on the lung volumes of the subjects or the exact flows during the washout.[43] Therefore, slow and rapid washout tests have been simulated using the lung volume and the regional pressure-fractional volume relations of the subject whose lung volumes were used to produce the simulations shown in Figures 5-11 and 5-12. The calculated Xe washout curves are shown in the top part of Figure 5-13. The slow washout has a flow of approximately 200 $cm^3 \cdot sec^{-1}$ and the rapid washout has a flow of approximately 2000 $cm^3 \cdot sec^{-1}$. This flow is reduced as a lung volume approaches RV in order to keep the pressure changes in the conducting airways in the physiological range. The Xe concentrations in the first 750 cm^3 of exhaled gas are not shown since the model only represents the emptying of the well mixed alveolar gas, not the initial gas where diffusion plays a role. The regional Xe concentrations at TLC are set up in the simulations and experiments by slowly inhaling a bolus at RV, which places most of the Xe in the apical regions (see Figure 5-11). The washouts are expressed as a function of exhaled volume, which is expressed as a % VC.

During the slow washout, the calculated Xe concentration at the mouth slowly increases, then shows a rapid rise once approximately 80% of the VC has been exhaled. This rise at the end of the washout is caused by the closure of airways in the basilar regions and the resulting decrease in compliance. As the compliance of the lower regions decreases the upper regions provide more of the gas to the expirate which causes the concentration of Xe at the mouth to increase. When the exhalation rate is rapid, the model predicts the lung will empty more uniformly, the Xe concentration at the mouth is more uniform and actually takes a dip at approximately 75% VC. At the very end of the rapid exhalation, a rise in the Xe concentration occurs.

Figure 5-12. Xe Concentration at the End of Inhalation (TLC) for a Xe Bolus Inhaled Slowly and Rapidly at 55% VC.

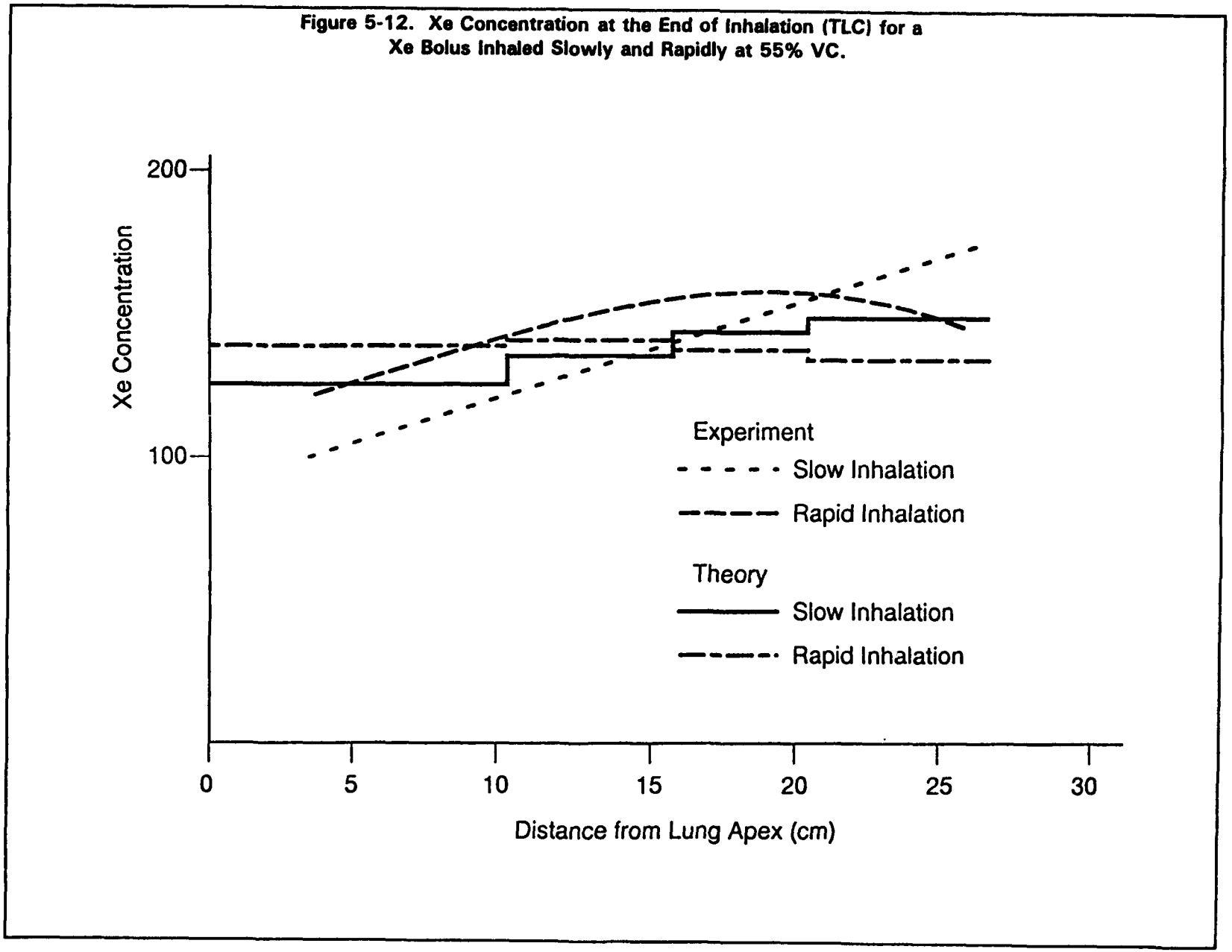

Figure 5-13. Top: Calculated Xe Washout Curves During Slow/Fast VC Exhalation. Bottom: Measured Xe Washout Curves During Slow/Fast VC Exhalation.

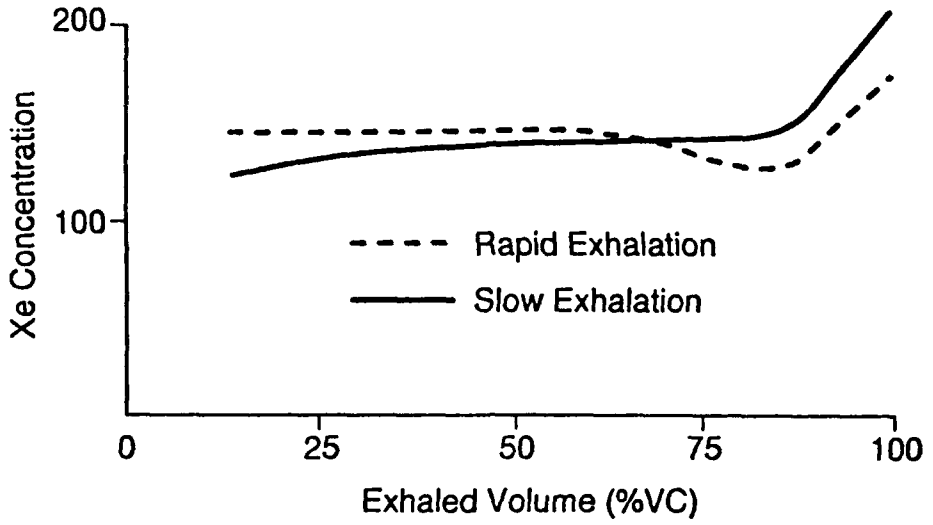

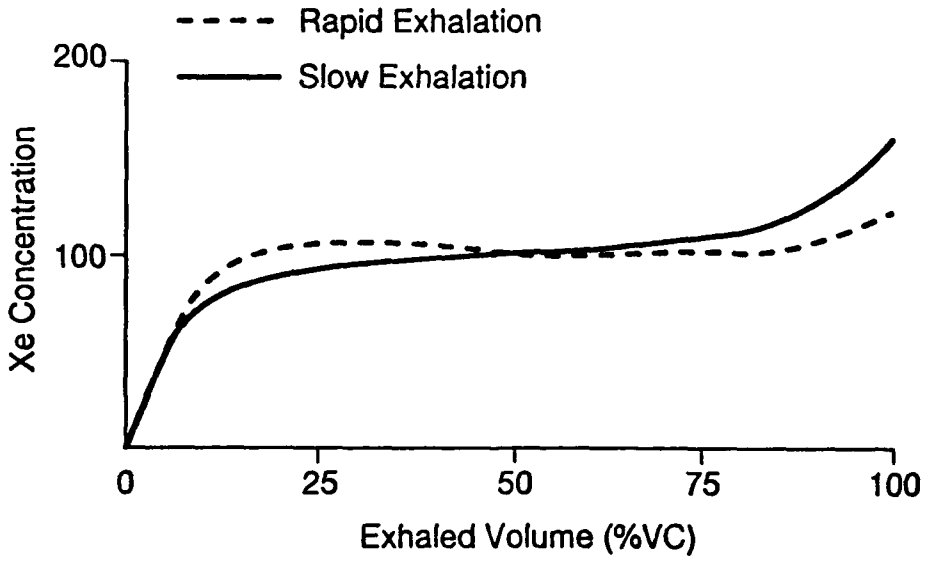

The measured curves are shown in the lower part of Figure 5-13. The relative positions of the measured slow and rapid wash out curves are similar to the relative positions of the calculated slow and rapid wash out curves. The emptying pattern of the Ventilation Model appears to qualitatively represent the emptying pattern of human lungs during the rapid exhalations.

5.3 The Convection-Diffusion Model.

5.3.1 Geometry of the Model.

The dimensions of the trumpet channel are obtained from the Weibel's Symmetric Lung Model A. The anatomical data is given as airway length per generation (l_n), diameter of each generation (d_n), number of airways per generation (naw_n) and the alveolar volume per generation ($Valv_n$) (see Table 5-1). The last 2.2 cm of the trumpet channel that represents Weibel's Symmetric Lung Model A is shown in Figure 5-14. The Y axis is the total cross-sectional area of all the airways and the X axis shows the distance from the trachea. The most important aspect of the trumpet channel in Figure 5-14 is the large cross-sectional area at the distal end of the trumpet. Over 90% of the volume is contained in the last centimeter of the channel. The cross-hatched area indicates the alveolar volume in each generation.

The alveoli are not situated on the conducting airways as individual sacs, instead they are found in groups with each group being connected to the conducting airway by a structure called a sac.[44] Figure 5-15 shows a schematic drawing of a sac with its attached alveoli, which is called an alveolar unit. All of the alveoli in the transport model are assumed to be arranged in alveolar units. There area of the sac opening is taken to equal 0.052 mm^2, the depth of the sac and its attached alveoli is 0.32 mm, the volume of the sac is 0.00454 mm^3 and the volume of each alveolus is 0.00392 mm^3.[44] If all of the alveoli are assumed connected to sacs there are 4.65 alveoli per sac and the volume of the alveolar unit equals 0.02671 mm^3. The total area of the sac openings per generation (Aso) equals the sac opening area multiplied by the number of sacs per generation.

The anatomical lung data in Weibel's Symmetric Lung Model A represents a lung volume of 4,820 cm^3 and this data is scaled to the starting lung volume of the subject whose breath is being simulated. The scaling is performed assuming the lengths changes are proportional to the cube root of the volume change.[39] The reference dimensions define the anatomical state of each region at the start of inhalation. During a breath each region inflates and deflates uniformly in three dimensions. The breathing process can be pictured as the movement of air into and out of each regional channel as the channel shown in Figure 5-3 expands and contracts. The dimensions of the channel at each new regional volume are obtained by multiplying the reference dimensions by the correct power of the cubic scaling factor.

Figure 5-14. Distance From the Trachea vs. the Log of the Total Cross-Sectional Area Over the Distal Most 2.2 cm of the Model.

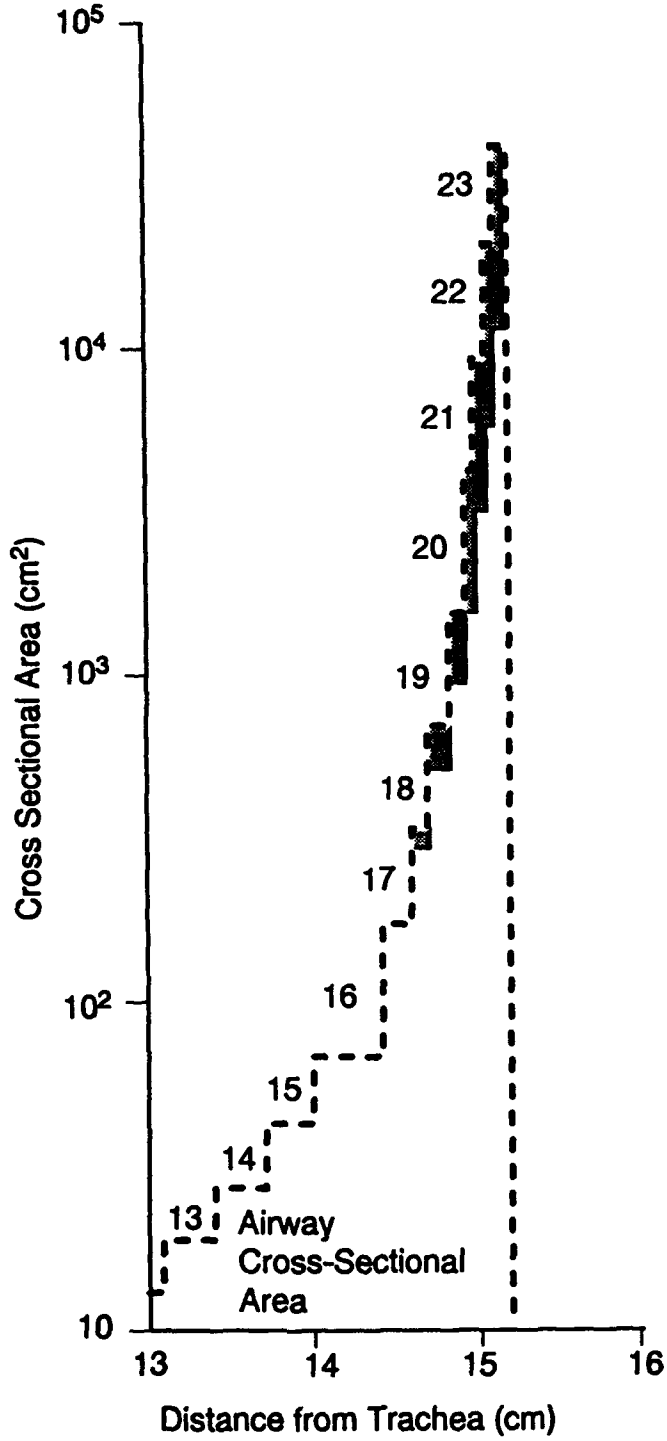

$$s = \left(\frac{Vi}{Vi_{ref}}\right)^{\frac{1}{3}} \qquad [5\text{-}27]$$

where Vi is the volume of the ith region and V_{ref} is the reference volume of the ith region. Therefore, at a given volume Vi with a scaling factor s, the length per generation is sl_n, the diameter is sd_n, the area of the channel is s^2A_n, the alveolar volume per generation is s^3Valv_n and the area of the sac openings per generation is s^2Aso_n, where the n subscript indicates the airway generation number.

Figure 5-15. An Alveolar Unit Consists of a Sac and Its Attached Alveoli. The Sac Connects the Alveoli to the Conducting Airway.

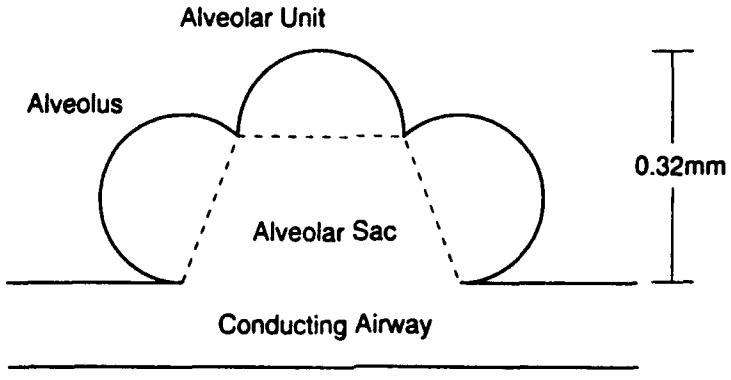

5.3.2 Convection-Diffusion Transport Equation.

The mass balance for a tracer gas in a channel with a cross-sectional area of s^2A can be established by considering a differential element of the trumpet channel with the length Δx as shown in Figure 5-16.

The rate of change of tracer gas in the element is given by

$$\frac{\partial}{\partial t}(s^2AC\Delta x) \ , \qquad [5\text{-}28]$$

which must equal the net gas flux of tracer gas into the element. Mathematically this corresponds to the following equation

Figure 5-16. Differential Element of the Trumpet Shaped Channel. The Fluxes of Tracer Gas Into and Out of the Channel are Shown.

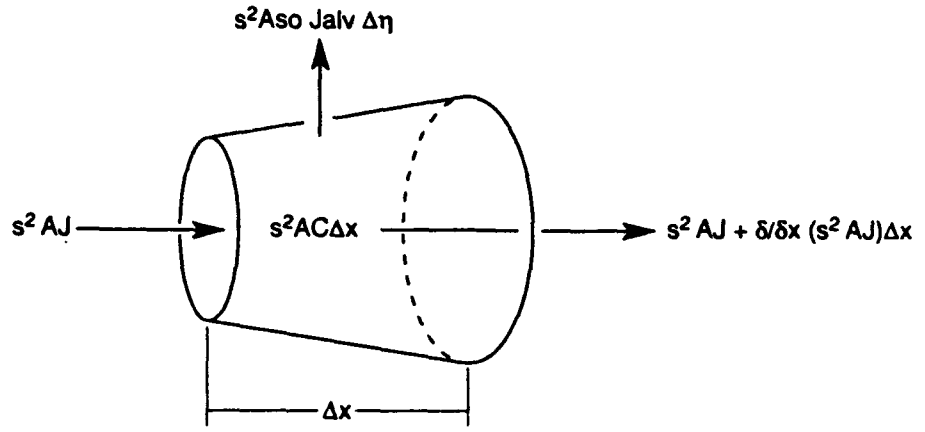

$$\frac{\partial}{\partial t}(s^2 A(x) C(x) \Delta x) =$$

$$\frac{\partial}{\partial x}(s^2 A(x) J(x) \Delta x) - s^2 Aso(n) Jalv(x) \Delta n \qquad [5\text{-}29]$$

where t represents time, C the airway concentration, J the axial gas flux in the airway, Jalv is the gas flux into the alveolar unit, n is the generation number and Δn equals Δx divided by *sl*, the fraction of an airway generation in the Δx segment. For convenience, time has not been listed as an independent variable in Equation 5-29, but it should be noted that C, J, Jalv, and s are all functions of time. The flux in the channel is given by

$$J(x) = U(x) C(x) - Dm \frac{\partial C(x)}{\partial x} \qquad [5\text{-}30]$$

where the axial velocity

$$U(x) = \frac{Q(x)}{s^2 Acx} \quad , \qquad [5\text{-}31]$$

where Q is the gas flow in the conducting airways and Dm is the molecular diffusion coefficient. Again time has not been listed as an independent variable but Q is a function of time. Substituting Equation 5-30 into Equation 5-2

$$\frac{\partial}{\partial t}(s^2 A(x) C(x) \Delta x) =$$

$$\frac{\partial}{\partial x}(s^2 A(x)\, Dm \frac{\partial C(x)}{\partial x} - Q(x)\, C(x)\, \Delta x - s^2\, Aso(x)\, Jalv(x)\, \Delta n \qquad [5\text{-}32]$$

Conservation of tracer gas in the alveolar region is specified by

$$\frac{\partial}{\partial t}(s^3\, Valv\, Calv) = s^2\, Aso\, Jalv \qquad [5\text{-}33]$$

where Calv is the average tracer gas concentration in the alveolar gas of a generation. The flux of tracer gas into the alveolar volume is

$$Jalv = \frac{Qalv}{(s^2 Aso)} Cso - Dm(\frac{\partial C}{\partial r})_{so} \qquad [5\text{-}34]$$

where Qalv is the flow into the alveolar volume, Cso is the gas concentration at the sac opening and Dm is the molecular diffusion coefficient, and

$$(\frac{\partial C}{\partial r})_{so} \qquad [5\text{-}35]$$

is the radial concentration gradient at the sac opening. Conservation of air volume in the alveolar unit requires that

$$Qalv = \frac{dValv}{dx} \; . \qquad [5\text{-}36]$$

To make the problem tractable, two assumptions are made concerning the tracer gas flux into the alveolar unit. First, the radial dependence is eliminated by approximating the radial concentration gradient at the sac opening with

$$\left(\frac{\partial C}{\partial r}\right)_{so} = \frac{Calv - C}{s\left(\frac{d}{2} + SD\right)/2} \qquad [5\text{-}37]$$

Secondly, the concentration at the sac opening is assumed to be the average of the airway concentration C and the alveolar concentration Calv, Cso = (Calv+C)/2. Substituting these equations into Equation 5-16, the transport into the alveolar region is

$$s^2 Aso\, Jalv = \frac{\partial}{\partial t}(s^3 Valv\, Calv) =$$

$$Qalv\frac{(C + Calv)}{2} - s\, Aso\, Dm\frac{Calv - C}{\left(\frac{D}{2} + \frac{sD}{2}\right)} \qquad [5\text{-}38]$$

Due to the complexity of the coefficient in Equations 5-32 and 5-38, these equations are solved numerically using finite differences. The breath is divided into small time increments Δt which correspond to the time increments used in the numerical calculation of the regional flows by the Ventilation Model. The gas concentrations are numerically calculated in each region at each axial position at the end of each time increment.

In order to solve the differential equation, initial conditions and boundary conditions are required. The initial condition is simply the tracer gas concentration in the lung before inhalation starts. At the distal end of the model a no-flux boundary condition is imposed as no tracer gas can pass through the back wall of the trumpet channel shown in Figure 5-2. During inhalation, the concentration of the tracer gas at the end of the trachea provides the boundary condition at the entrance to the channel, but this concentration is not known and must be calculated as a function of time. In order to do this, the mouth and pharynx are treated as an extra length added to the trachea which is represented as a rigid tube of constant cross-sectional area. Equation 5-32 gives the mass balance in this tube with Jalv = 0. This differential equation is solved numerically in order to calculate the concentration of the tracer gas at the end of the trachea, the entrance to the four trumpet channels that form the Convection-Diffusion model.

5.3.3 Results and Validation.

Figure 5-17 shows the data collected during a single breath N_2 washout test (N_2 fractions are dry gas fractions) as well as the concentrations calculated at the mouth during exhalation in the simulation performed with the Pulmonary Model. In a single breath N_2 washout test, a subject, starting at a preset lung volume, inhales a tidal volume of gas that is low in N_2, usually pure O_2, then exhales to RV. During exhalation the N_2 concentration at the mouth is

measured and the plot of N_2 concentration vs. exhaled volume (or time) is called the washout curve. In this simulation, the measured flows were used as an input in the Ventilation Model. The regional flows and volumes from the Ventilation Model were input into the Convection-Diffusion Model and the N_2 concentration throughout the four regions was calculated. The subject that performed this single breath N_2 washout test had an RV = 1600 cm^3 and a TCL = 7040 cm^3.

The calculated N_2 washout profile compares well with the measured N_2 washout curve. The gas originally in the instrument deadspace, the mouth, pharynx and trachea is the first gas to enter the lungs. Once this deadspace gas has been inhaled fresh tidal gas starts to enter the lungs and a front is quickly established between the inhaled gas which has a low N_2 concentration and the resident gas which has a high N_2 concentration. Figure 5-18 shows the calculated concentration profiles at 1 sec intervals in Region 1 as a function of the summed volume along the center axis of the channel. The regional volume and the inhaled volume are given for each time in the inset.

As inhalation proceeds the N_2 concentration decreases as the alveolar gas in Region 1 is diluted with O_2, but the center of the front that separates the low and high concentration N_2 gas remains near 50 cm^3 (generation 15) during the entire inhalation period. The axial position of the front is determined by the cross-sectional area of the trumpet channel and the flow rate. The front is at the position where the N_2 transport by convection into the region is equal and opposite the transport by diffusion out of the region, i.e. the N_2 is convected into the region as fast as it diffuses mouthward. In the airways located mouthward of generation 16, the cross-sectional area of the channel is small and the large gas velocities in these generations makes convection the dominant transport mechanism. In the generations located distal to the front, the channel has a very large cross-sectional area and molecular diffusion is the dominant transport mechanism.

During inhalation, a small concentration gradient exists in the first 500 cm^3 of the alveolar gas in Region 1, but the gas located distal to this position is completely mixed. Molecular diffusion quickly reduces the concentration gradients that are created by the influx of O_2 into the deep alveolar gas. The combination of the large cross-sectional areas and the short lengths of each generation enables molecular diffusion to be so effective. The distance along the center axis of the channel between a volume of 50 cm^3 and the distal end of the channel is only 1 cm.

When exhalation starts convection no longer opposes diffusion and both mechanisms transport the N_2 mouthward. This coupling of convection and diffusion quickly eliminates any concentration gradients in the alveolar gas in Region 1. This is seen in Figure 5-18 at t=4 sec. After 44 cm^3 of gas have been exhaled a non-negligible concentration gradient exists in only the first 150 cm^3 of gas, the other 1170 cm^3 of gas in the region are completely mixed. At t=5 sec the region has exhaled only 127 cm^3 of gas, but all of the remaining gas is completely mixed, there are no concentration gradients within the region. The situation in the other three regions is similar, except the N_2 concentrations are lower because the

ventilation to volume ratio is higher in the more dependent regions (see Figure 5-10). This means that more gas low in N_2 enters these regions, reducing the alveolar N_2 concentration below those seen in Region 1.

While the agreement between the measured and calculated curve in Figure 5-18 is good, it turns out that the use of four compartments has little affect on the N_2 washout because the vertical N_2 concentration differences are relatively small. A single region would have produced an almost similar washout curves, but the regional differences are important in determining the alveolar gas concentration, which will be important when the model is expanded to include transport between the blood and alveolar gas.

Figure 5-17. Experimental Recordings Showing the N_2 Fraction and Flow Measured at the Mouth, and the Inhaled/Exhaled Volumes.

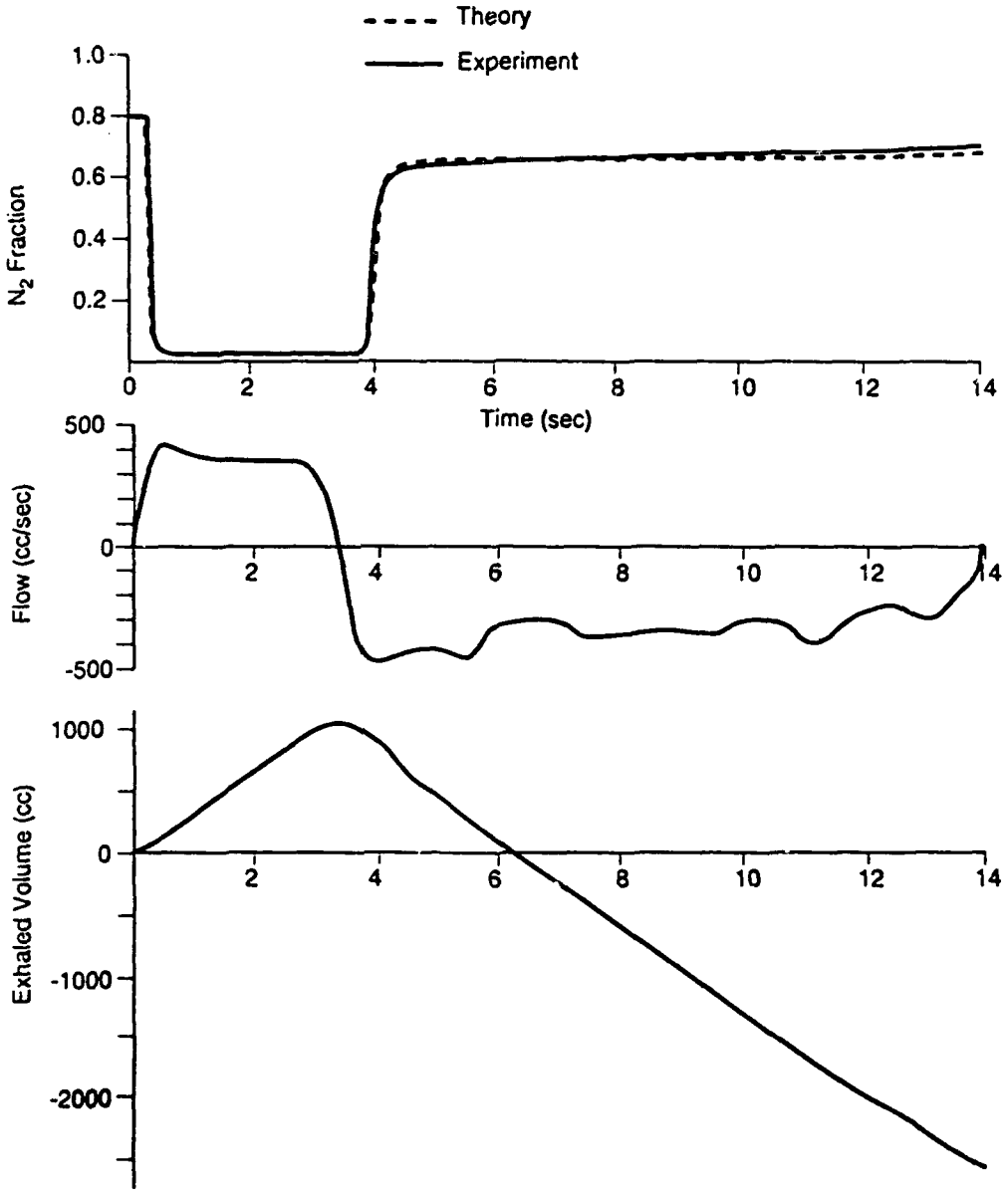

Figure 5-18. Calculated N_2 Fraction in Region 1at 1Sec Intervals and at the End of Inhalation (3.4 Sec). X-Axis Is Summed Volumes Along the Center Axis of the Channel that Represents Region 1.

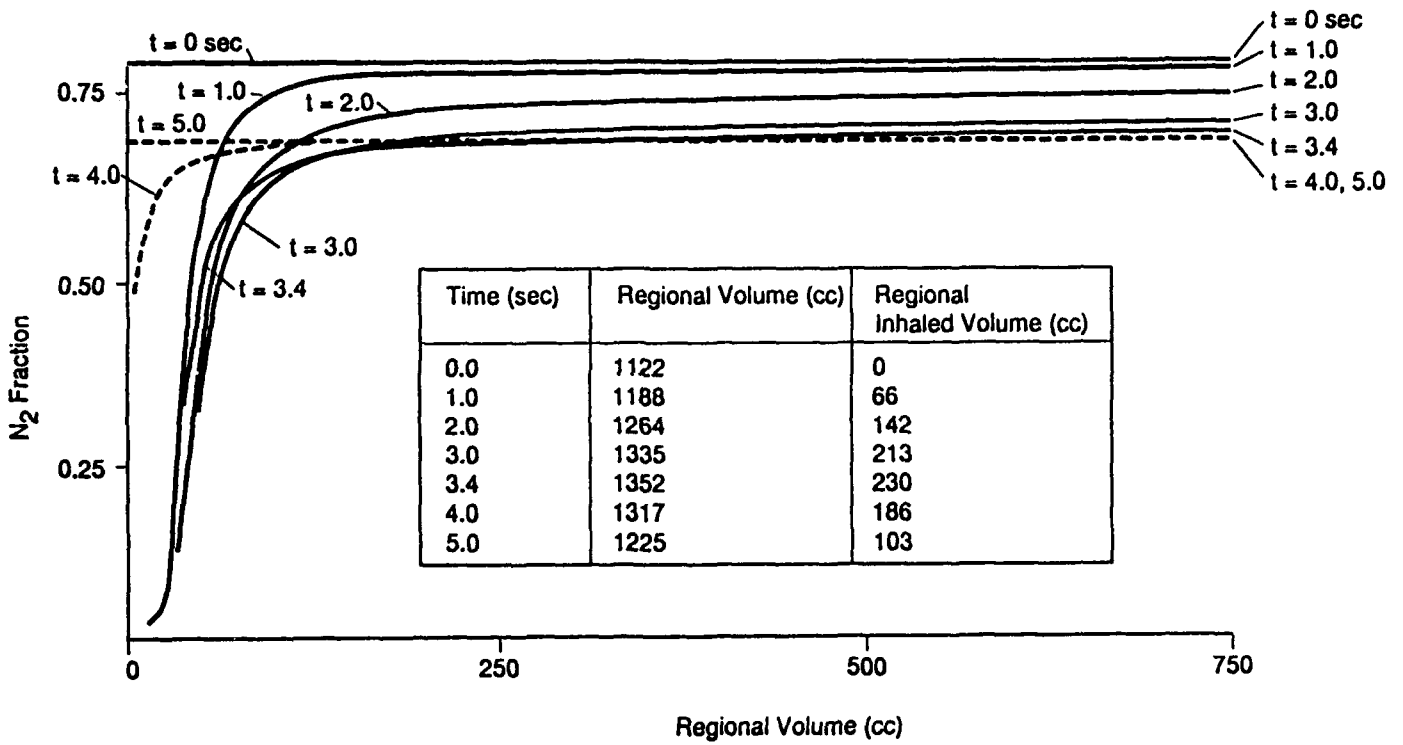

Time (sec)	Regional Volume (cc)	Regional Inhaled Volume (cc)
0.0	1122	0
1.0	1188	66
2.0	1264	142
3.0	1335	213
3.4	1352	230
4.0	1317	186
5.0	1225	103

SECTION 6.0

6.0 Cardiovascular Model.

6.1 General Description.

As stated previously, the cardiovascular model described herein parallels the development presented in a paper by White, et al.,[18] as well as papers by Jaron, et al.,[19,20,21] and earlier papers by Rideout,[22] Snyder,[23] and Avula.[24] Many of the parameter values for the physical properties of the vascular segments were taken from these papers as well as Fung[45] and Bergel.[46] However, some of the parameters listed in Jaron[19] were clearly in error and some of those employed by other authors were not useful because of differences in the layout of their models and ours. Where new parameters were required, they were derived to yield generally acceptable flow/pressure/volume and compliance characteristics of the various cardiovascular subdivisions. In particular, flow, pressure, and compliance data from Burton,[47] and Guyton,[48] were employed.

Figure 6-1 displays the general schematic for the model compartments and their connections.

It appears feasible and desirable to extend the Phase I model in Phase II to include the short term physiologic control and the effects of pressure breathing on cardiovascular flows and pressures. This will enable the model to more faithfully simulate the true response of the cardiovascular system in response to short term changes in acceleration and breathing rate, depth, and pressure. An enhanced Phase II cardiovascular model could be validated against experimental data and then employed to estimate the physiologic effects of changes in the operating conditions of the breathing system.

6.2 System Equations.

The model describes the spatial and temporal variation in the mean blood pressure along the z-axis of the body. The present implementation neglects the non-linear and convective terms in the Navier-Stokes Equation as well as the complication of radial flow (flow perpendicular to the vessel wall). The flow is assumed to be laminar except in the ascending an descending aorta where fluid flow resistances were multiplied by 33 to account for increased pressure losses in turbulent flow.[21] The following set of coupled differential equations were solved for each arterial and venous vascular segment.

$$\frac{dP(t)}{dt} = \frac{1}{C}\cdot(Q(t)_{in} - Q(t)_{out}) + R_w\cdot(Q(t)_{in} - Q(t)_{out}) \qquad [6\text{-}39]$$

$$\frac{dQ(t)}{dt} = \frac{1}{L}\cdot(P(t)_{in} - P(t)_{out} + P_{G_z} - R\cdot Q(t)) \qquad [6\text{-}40]$$

Figure 6-1. Cardiovascular System Model Compartments and Connections

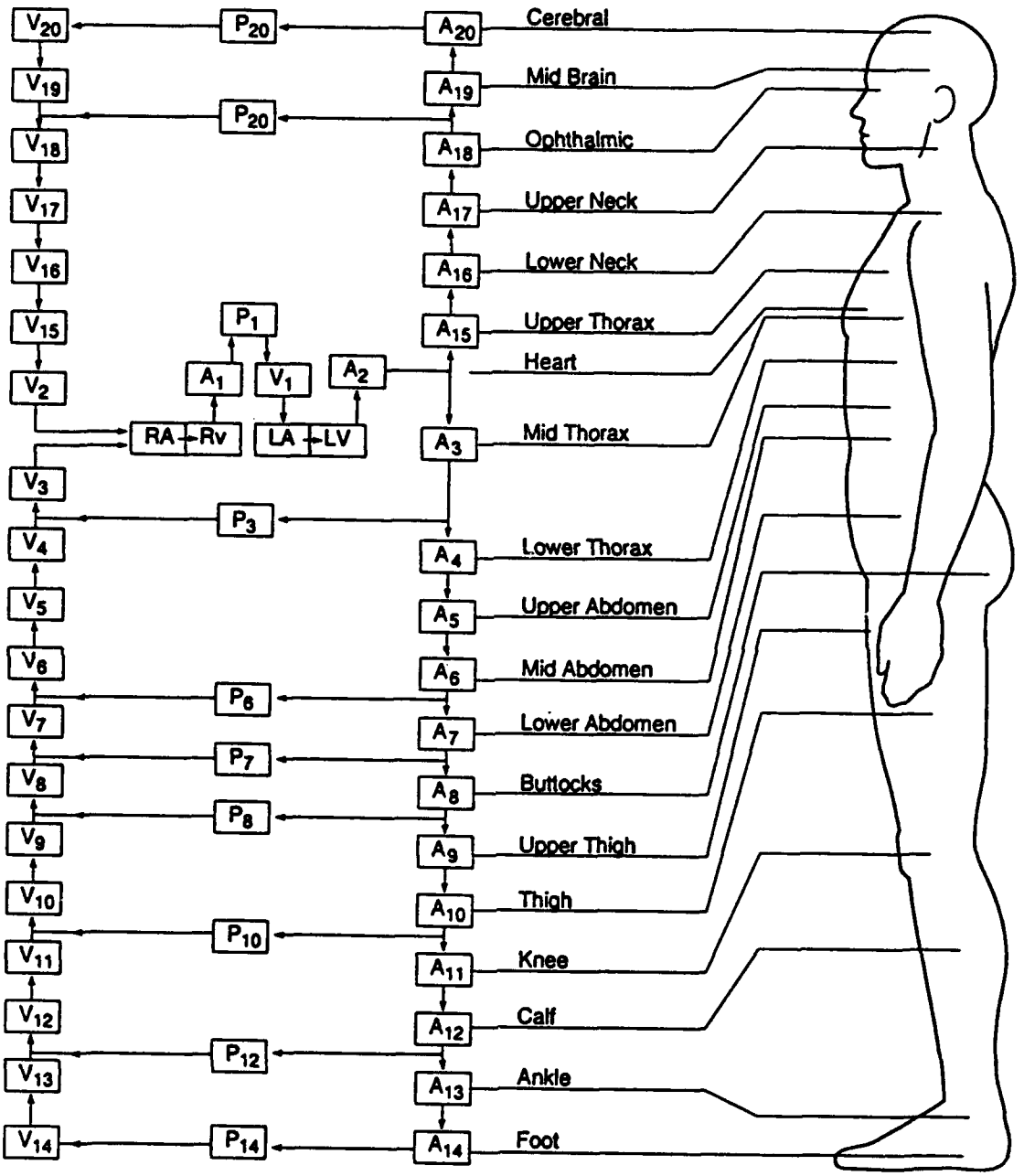

$$\frac{dr(t)}{dt} = \frac{1}{2 \cdot \pi \cdot r(t) \cdot l} \cdot (Q(t)_{in} - Q(t)_{out}) \qquad [6\text{-}41]$$

Where,

t	= Time	[sec].
r	= Radius of vascular segment	[m].
l	= Length of vascular segment	[m].
P	= The pressure in the segment	[Pa].
Q	= The segmental volume flow	[$m^3 \cdot sec^{-1}$].
C	= The capacitance of the segment	[$m^3 \cdot Pa^{-1}$].
L	= The inertance of the segment	[$kg \cdot m^{-4}$] or [$Pa \cdot sec^2 \cdot m^{-3}$]
R	= The viscous flow resistance in the segment	[$Pa \cdot sec \cdot m^{-3}$].
R_w	= The vessel expansion resistance	[$Pa \cdot sec \cdot m^{-3}$].
P_{Gz}	= The hydrostatic pressure difference across the segment because of gravity	[Pa].

And, the following approximations for R, L, and C were taken from Rideout, et al.[5]

$$R = \frac{81 \cdot \mu_0 \cdot l}{8 \cdot \pi \cdot r^4} \qquad [6\text{-}42]$$

$$L = \frac{9 \cdot \rho_0 \cdot l^2}{4 \cdot V} \qquad [6\text{-}43]$$

$$C = \frac{3 \cdot r \cdot V \cdot l}{2 \cdot E \cdot h} \qquad [6\text{-}44]$$

$$R_w = \frac{0.002}{C} \qquad [6\text{-}45]$$

Where,

E	= Young's modulus for vessel wall	[Pa].
h	= Vessel Wall thickness	[m].
ρ_0	= density of blood	[$kg \cdot m^{-3}$].
μ_0	= viscosity of blood	[$N \cdot sec \cdot m^{-2}$].

Finally,

$$P_{G_z} = \rho_0 \cdot G_z \cdot g_0 \cdot l \cdot Cos(\theta) \qquad [6\text{-}46]$$

Where,

G_z = The z-axis "G-level" in units of earth's gravity [unitless]
g_0 = The earth's gravitational acceleration [$m \cdot sec^{-2}$]
θ = The angle between the segment and the z-axis [radians].

For each vascular segment, Equations 6-39, 6-40, and 6-41 must be solved simultaneously. There are 20 arterial and 20 venous vascular segments (the pulmonary circuit is segment 1). There are 10 peripheral capillary bed segments modelled by differential equations for pressure and flow. The peripheral capillary resistance and capacitance are modelled as "T" circuits with the peripheral capacitance in parallel with an inlet and outlet resistance which represent the resistance of the arteriole and venule respectively. The pulmonary circulation is modelled as a single peripheral bed fed by a single arterial segment and drained by a single venous segment. The chambers of the heart are modelled as variable capacitances separated by one-way valves. The pulmonic and aortic valves are also modelled as one-way valves. The pressure reference for the model is located at the tricuspid valve which is presumed to track intrathoracic pressure. The pressures and flows in the various segments are coupled by their spatial connections. The z-axis coordinates for locating the origin and termination of each segment were based on a 177 cm tall standing man. Including the equations for pressure and flow in the heart, there are 174 differential equations in the model. The solution was computed using a Runge-Kutta numerical integration algorithm.[49]

6.3 Simulation Results.

The initial conditions for segmental flow were set based on a steady-state solution for the model at 1 G_x (transverse) corresponding to a supine posture. Initial pressures were set by computing the hydrostatic pressure at each segment corresponding to the initial local z-axis acceleration. Posture is adjusted by setting the appropriate initial orientation angle for each segment relative to the z-axis acceleration. Postural and acceleration changes during a simulation may be made by adjusting the orientation angles and/or acceleration during the simulation. This can be most easily accomplished by adding time varying profiles for G_z and the θ's from which the P_{Gz} values for the flow derivatives are calculated. However, the current version of the model does not include provisions for simulating the effects of the short term cardiovascular reflexes responsible for controlling the blood pressure and distribution of blood flow. Therefore, no attempt was made to match transient responses of the model to those expected in the response of the true cardiovascular system. Rather, the model was coded so that the cardiac output was maintained at a constant value (5.4 liters·min^{-1}) until the regional blood flow values returned to their initial values. The resulting steady-state pressures or "equilibrium pressures" in the various segments represent

the pressures required to maintain "normal" blood flow through the vascular and peripheral segments. The results of the two simulations described below illustrate the results of this process.

To illustrate the use of the model to estimate the effects of acceleration on the cardiovascular system, three simulations were conducted. Figures 6-2 and 6-3 present a comparison of the equilibrium arterial and venous pressures at $+1\ G_z$ at two different postures: upright and reclined. The segment numbers have been arranged so that the pulmonary segment (Segment 1) is at the far left and the remaining segments show the pressures beginning at the most headward segment (Segment 20) and ending at the most footward segment (Segment 14). The segment orientations for the reclined posture were chosen to approximate the seated posture in a high performance fighter cockpit with a seat back reclination angle of 20° with the feet and thighs slightly elevated in relation to the buttocks. The second set of simulation results is shown in Figures 6-4 and 6-5 which illustrate the equilibrium arterial and venous pressures in cardiovascular system for the reclined posture at two different acceleration levels: $+1\ G_z$ and $+4\ G_z$. As shown, at the elevated acceleration the more headward arterial segments are showing negative pressures.

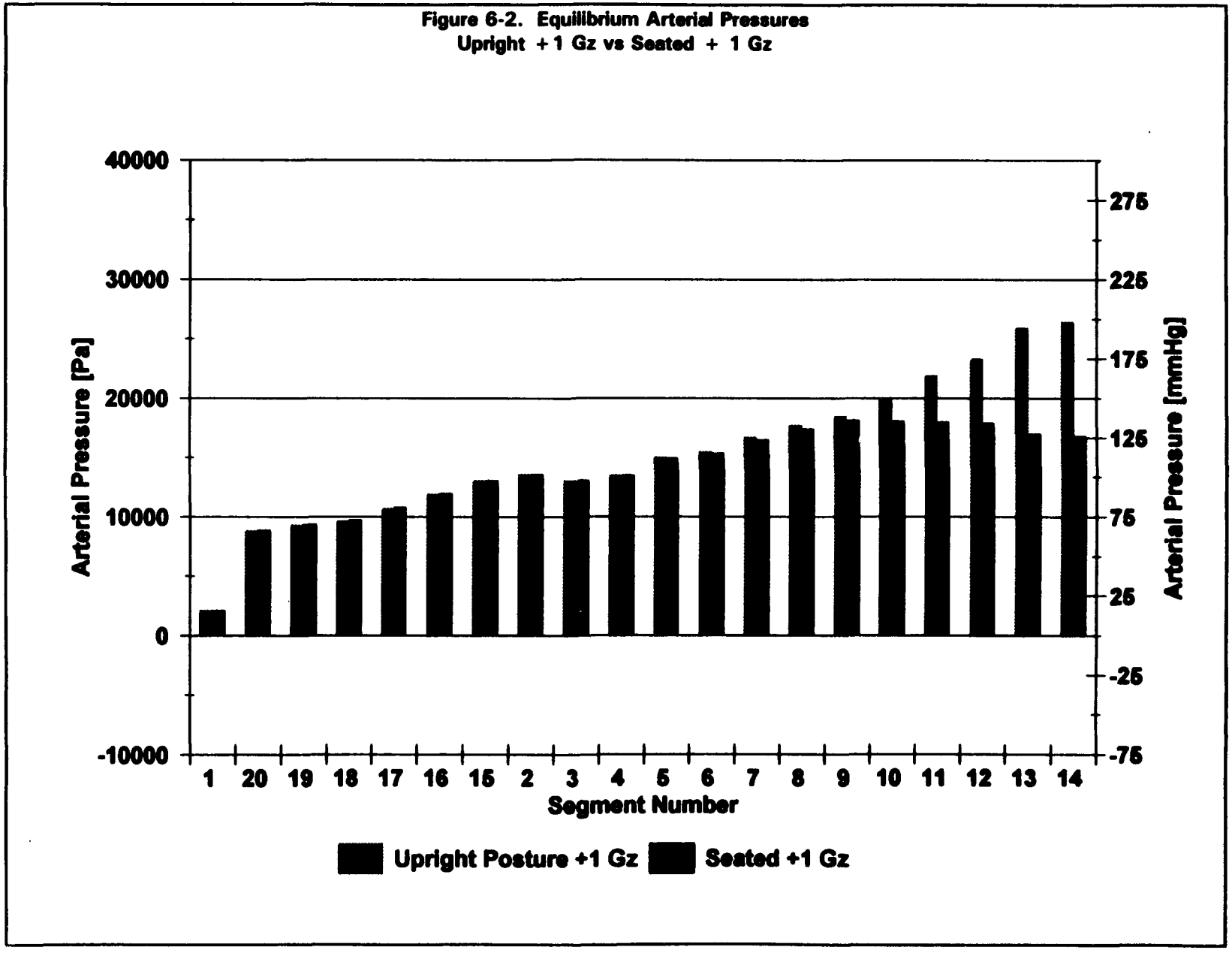
Figure 6-2. Equilibrium Arterial Pressures
Upright +1 Gz vs Seated + 1 Gz
Arterial Pressure [Pa]
40000
30000
20000
10000
0
-10000
Arterial Pressure [mmHg]
275
225
175
125
75
25
-25
-75
1 20 19 18 17 16 15 2 3 4 5 6 7 8 9 10 11 12 13 14
Segment Number
Upright Posture +1 Gz
Seated +1 Gz

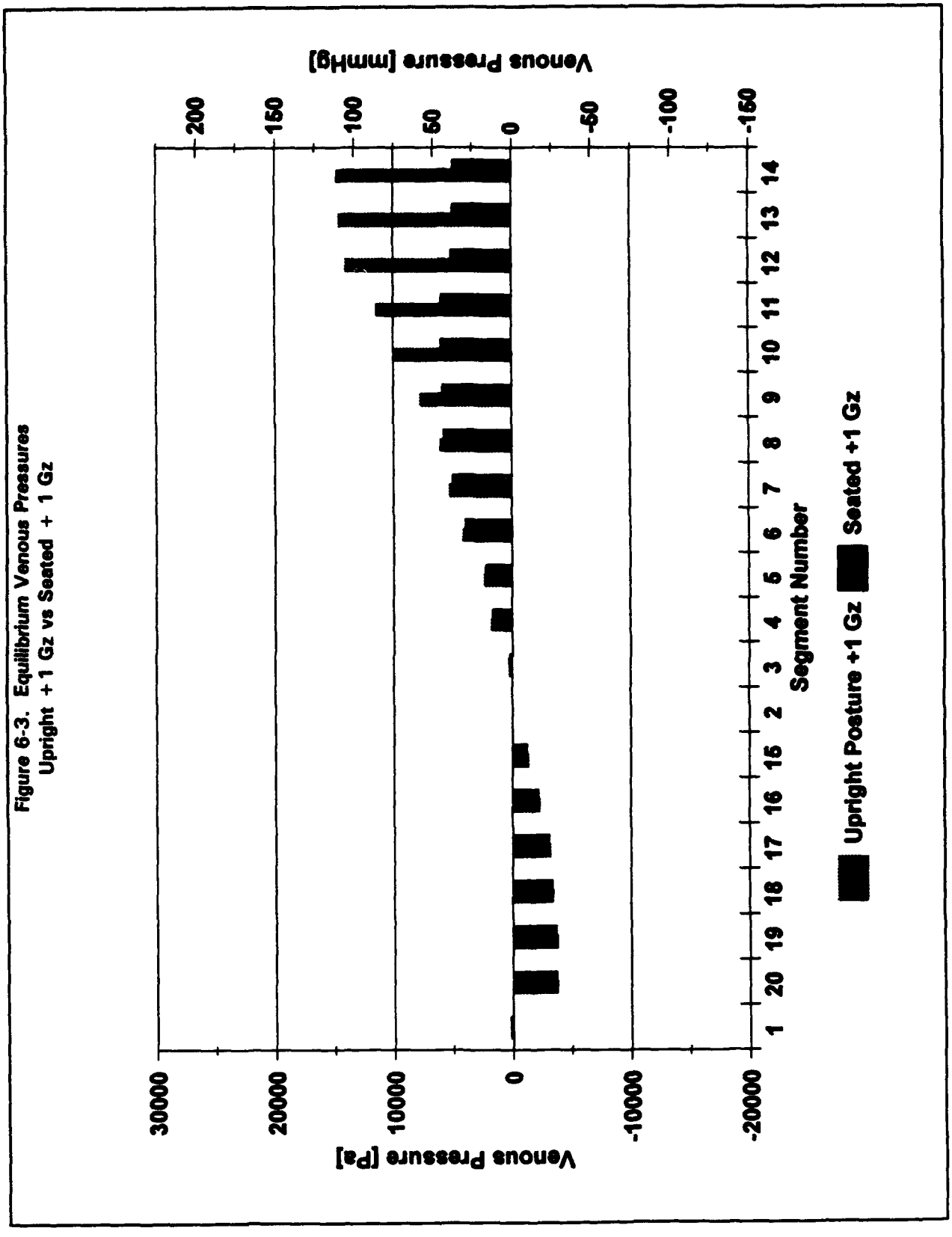

Figure 6-3. Equilibrium Venous Pressures
Upright +1 Gz vs Seated + 1 Gz

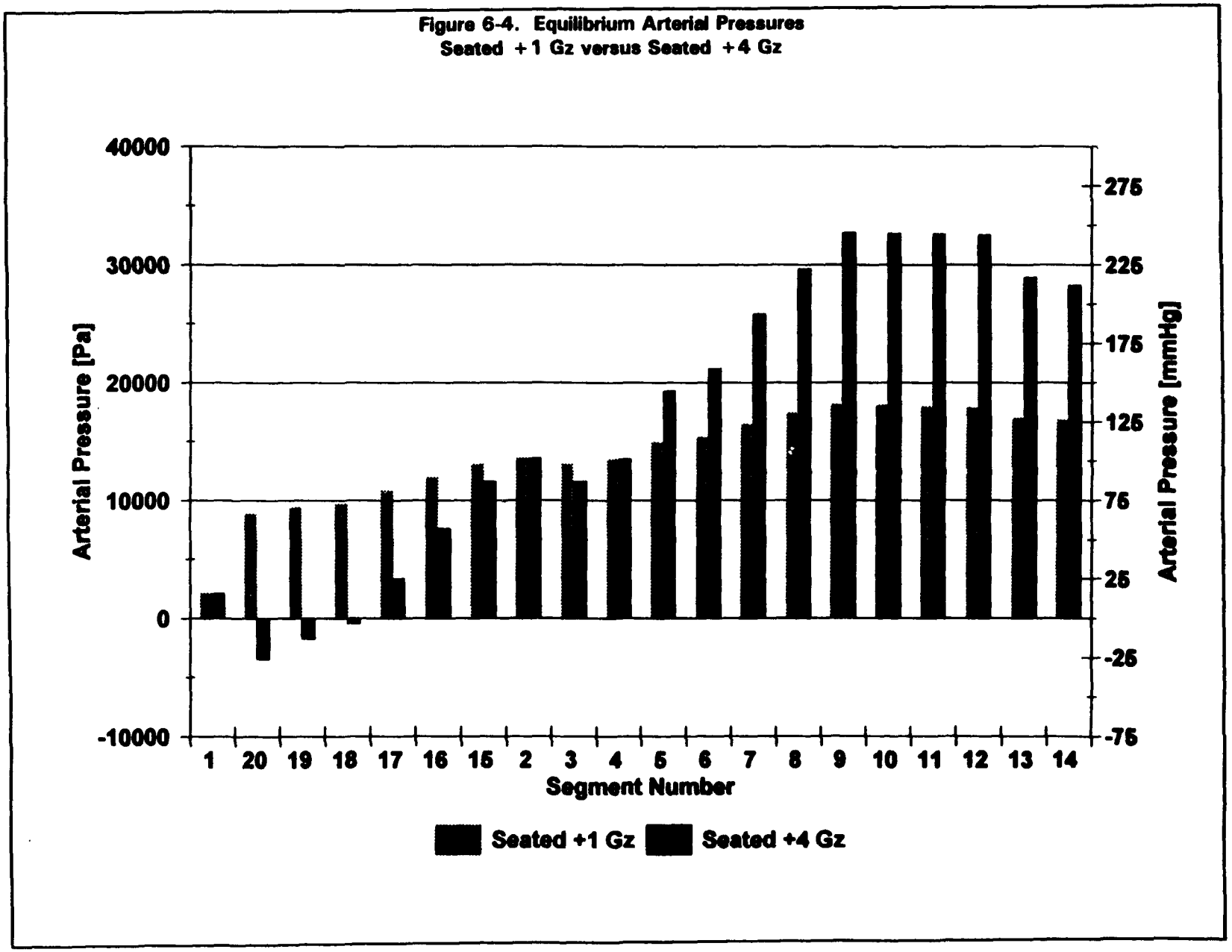
Figure 6-4. Equilibrium Arterial Pressures
Seated +1 Gz versus Seated +4 Gz
Arterial Pressure [Pa]
40000
30000
20000
10000
0
-10000
Arterial Pressure [mmHg]
275
225
175
125
75
25
-25
-75
1 20 19 18 17 16 15 2 3 4 5 6 7 8 9 10 11 12 13 14
Segment Number
Seated +1 Gz
Seated +4 Gz

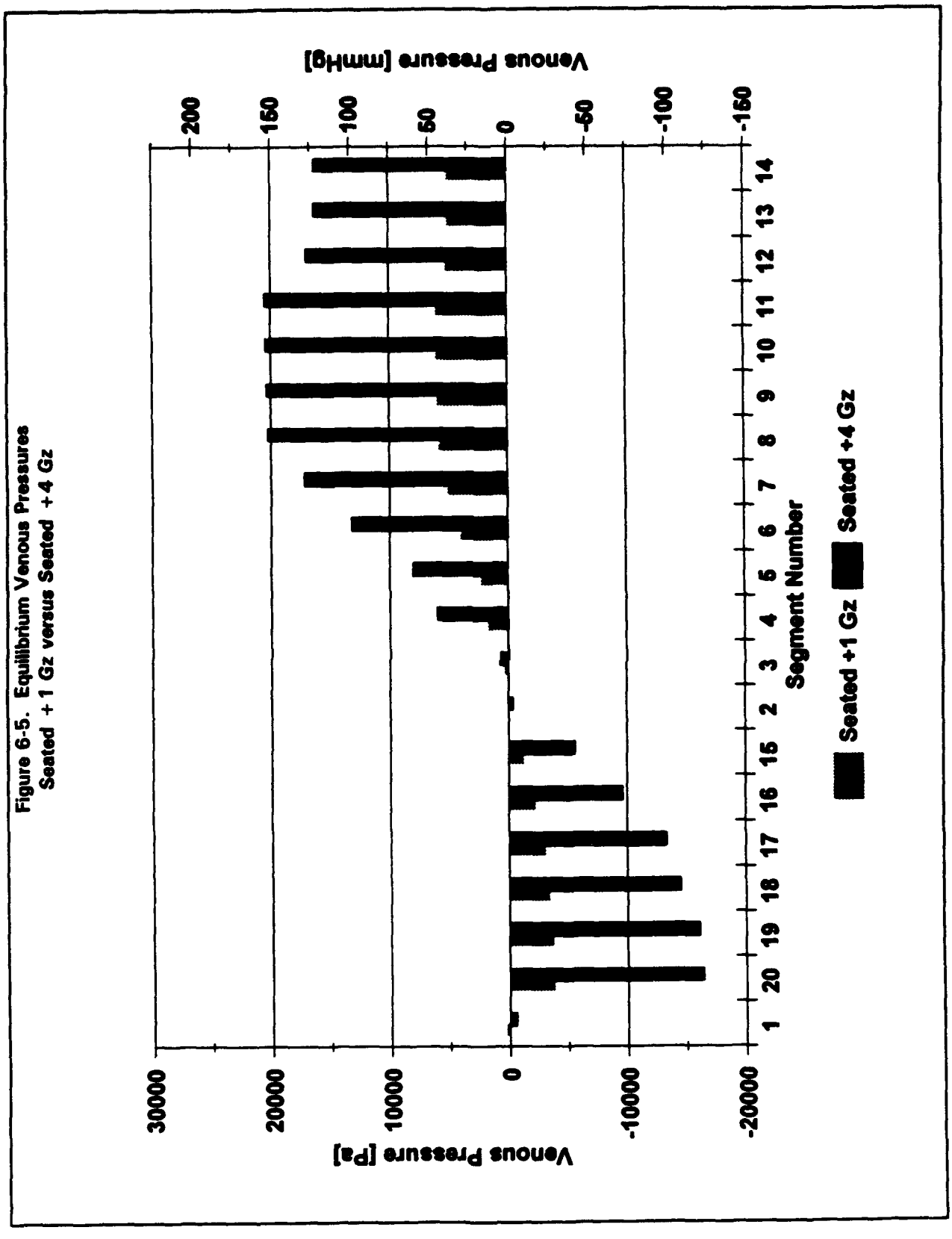

Figure 6-5. Equilibrium Venous Pressures
Seated +1 Gz versus Seated +4 Gz

SECTION 7.0

7.0 Physiologic Data and Validation.

7.1 Rapid Decompression Data.

BRC reviewed the rapid decompression data furnished by the Government. This series of experiments was referred to as the "EONS Experiments" because they were carried out to verify the US Navy's Expeditionary Oxygen Nitrogen System (EONS). The tests were designed to study the effect of breathing a gas mixture with less than the 98% oxygen at high altitude. The motivation for testing lower oxygen concentrations than found in Aviator's Breathing Oxygen (ABO) was to develop evidence that gas mixtures produced by Molecular Sieve Oxygen Generation Systems (MSOGS) were acceptable for use after rapid decompression to 50,000 feet (15.24 km) altitude. The studies were carried out during 1986-1988 in the Altitude Chambers at Brooks AFB, TX by the staff of the Crew Technology Division of the USAF School of Aerospace Medicine.

BRC obtained the raw data files and reviewed them for suitability as data for validating the ABS model. A total of 170 experimental data files were reviewed and assessed for quality. The data have been organized, cataloged, and collated by subject, by experimental condition, and by variable for easy review and access (See Appendix A). The Table 7-1 entitled, "EONS Flights" is a matrix that summarizes all of the test data. Each row of the table represents an individual test subject and each column represents the test number. Each element of the matrix contains the test date, the analog tape number, the digitized ASCII file name, and notes on test events. Spreadsheet files have been created in Quattro Pro which summarize the test data according to test subject and test number. Included in these files are time history plots of mask pressure, chamber pressure, partial pressure of oxygen and carbon dioxide, and inspiratory flow.

The test subjects wore standard USAF flight gear including a flight suit, anti-G suit, helmet and MBU-12P oxygen mask. The decompression profile consisted of a five minute exposure to 20,000 feet altitude while breathing either diluted or undiluted supply gas from a standard USAF CRU-73A Diluter-Demand Regulator. At the end of the five minute equilibration period, the chamber was decompressed to 50,000 feet in approximately 1 sec. The chamber altitude was then held for 1 minute before a descent to 40,000 feet was initiated. The data presented in the charts shows the time history of the recorded variables for a two minute period beginning one minute before the decompression and ending one minute after the decompression.

The respiratory variables recorded in the data files were inspiratory flow, mask cavity pressure, altitude chamber pressure, and the partial pressures of Oxygen (PO_2) and Carbon Dioxide (PCO_2) at the end of each breath (end-tidal). Thus, the data are not continuous, but are sampled from the original continuous analog tapes at the end of each breath. The inspiratory flow data were supplied as the peak inspiratory flow from the breath prior to the sampling time and as time averaged inspiratory flows from previous breaths ($\dot{V}_I$). The

time averaging was achieved with a three breath moving average filter. The inspiratory flow data plotted in the charts are the time averaged data, although both measures were included in the data files and spreadsheets. To illustrate the character of the data, examples of data from Subject BES are shown in Figure 7-1, below. In the graph, the abscissa is time in seconds, the left ordinate is absolute pressure and the right ordinate is flow. The chart title encodes the experimental conditions. In Figure 7-1, the data are displayed for subject BES, breathing undiluted 100% oxygen before and after the 5 psig decompression from 20,000 to 50,000 feet (6096 to 15240 m). The data show the chamber pressure and mask pressure falling immediately after the decompression begins. The chamber pressure falls to 88 mmHg while the mask pressure falls only to slightly over 110 mmHg because of the onset of 30 mmHg pressure breathing (PBA). The end-tidal PO_2 falls from approximately 260 mmHg before the decompression to 50 mmHg post decompression while the corresponding PCO_2's fell from approximately 35 mmHg to 30 mmHg. The inspiratory flow is seen to have risen briefly from about 7 liter·min^{-1} after the decompression and then return to the 15 to 20 liter·min^{-1} toward the end of the exposure.

Figure 7-1. Subject: BES/100% O2 Non-Dilution
20/50 kft Rapid Decompression

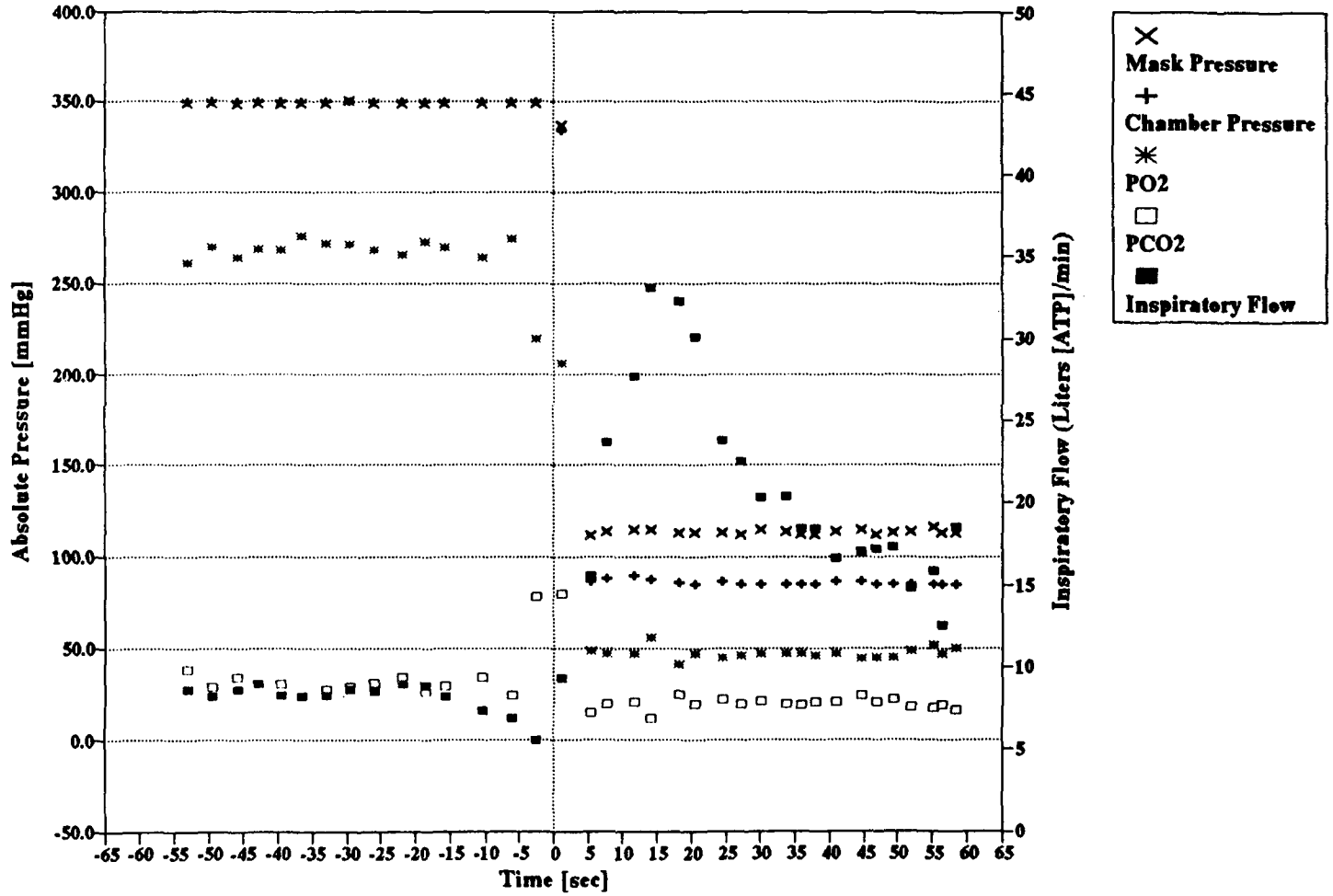

Table 7-1. EONS Flights

# Subject	1 A-100%	2 A5-100%	3 B-100%D	4 C-93%	5 D-93%D	6 E-90%	7 F-90%	8 G-85%	9 H-85%	10 EONS2
1 BES # Tape Notes File Name	3/11/87 1 7 BESAO	6/1/87 1 No Data 	5/22/87 1 13 BESBO	5/18/87 1 8 Small ML after RD BESCO	8/3/87 1 18 Lost MS for 5 sec after RD BESDO	4/27/87 1 11 BESEO	2/3/88 2 22,24 Small ML after RD BESFO	1/26/88 2 16,24 BESGO	2/12/88 2 22,25 BESHO	1/20/88 1 24 BES20
2 BOM # Tape Notes File Name	12/8/86 1 1 NOIF,A5, LOC at 2 min 	6/5/87 1 15 BOMAO	2/1/88 2 7,24 BOMBO	12/16/87 2 3,23 BOMCO	1/15/88 2 20,24 BOMDO	4/17/87 1 11 BOMEO	1/8/87 2 22,24 BOMFO	7/17/87 1 17 BOMGO	11/23/87 1 23 BOMHO	* 1 * No data on tape
3 COX # Tape Notes File Name	2/4/87 1 4 A5 	6/26/87 1 16 COXAO	4/10/87 1 10 COXBO	2/11/88 2 8,25 COXCO	8/26/87 1 20 COXDO	3/18/88 2 13,25 COXEO	12/15/87 2 21,23 COXFO	7/24/87 1 17 COXGO	11/30/87 1 23 COXHO	1/25/88 1 24 COX20
4 CRI # Tape Notes File Name	3/16/88 3 7,24,25 CRIAO	5/18/87 1 13 LOC just before descent CRIBO	4/8/87 1 10 CRICO	2/1/88 2 8,24 CRIDO	8/5/87 1 19 CRIEO	6/3/87 1 15 CRIFO	10/6/87 1 22 CRIGO	7/27/87 1 18 CRIHO	12/16/87 1 23 CRI20	2/23/87 1 5

RD = Rapid Decompression, ML = Mask Leak, MS = Mask Spec, LOC = Loss of Consciousness

# Subject	1 A-100%	2 A5-100%	3 B-100%D	4 C-93%	5 D-93%D	6 E-90%	7 F-90%	8 G-85%	9 H-85%	10 EONS2
5 DOA # Tape Notes File Name	1/26/87 ML, did not analyze	4/13/87 Did not analyze	1/21/88 3 6,23,24 ML, LOC ? DOABO	2/27/87 1 4 Tc prob, ML	6/10/87 1 15 DOADO	2/26/88 2 13,25 ML DOAEO	3/14/88 2 20,25 ML DOAFO	7/15/87 1 17 ML DOAGO	9/11/87 1 22 DOAHO	2/9/87 1 4 ML DOA2O
6 HAT # Tape Notes File Name	3/4/87 1 6 A5	6/15/87 1 16 HATAO	5/27/87 1 13 Did not analyze, ML	4/11/87 1 9 HATCO	10/28/87 1 22 HATDO	8/17/87 1 19 HATEO	4/7/88 1 26 HATFO	12/1/87 1 23 HATGO	Incomplete	2/11/87 1 5 ML after RD, analyzed HAT20
7 HIL # Tape Notes File Name	7/31/87 1 18	12/10/87 1 23,50 ML after 150 HILAO	1/25/87 1 23 ML after 20, did not analyze	8/19/87 1 19 HILCO	3/18/87 1 25 HILDO	9/10/87 1 22 HILEO	4/1/88 1 25 HILFO	1/19/88 1 24 HILGO	Incomplete	Incomplet e
8 HOS # Tape Notes File Name	8/28/87 1 20	2/25/88 1 25 HOSAO	1/28/88 1 24 Did not analyze	11/9/87 1 22 Did not analyze	3/11/88 1 25 HOSDO	12/7/87 1 23 ML after ? HOSEO	3/28/88 1 25 HOSFO	3/25/88 1 25 HOSGO	4/6/88 1 26 HOSHO	Incomplet e

RD = Rapid Decompression, ML = Mask Leak, MS = Mask Spec, LOC = Loss of Consciousness

# Subject	1 A-100%	2 A5-100%	3 B-100%D	4 C-93%	5 D-93%D	6 E-90%	7 F-90%	8 G-85%	9 H-85%	10 EONS2
9 JAR # Tape Notes File Name	12/10/86 1 2 NOIF, A5 	7/24/87 1 17 JARAO	6/30/87 1 16 	3/25/87 2 2,8 JARCO	8/10/87 1 19 JARDO	11/30/87 1 23 JAREO	4/5/88 1 25 Bad ML, did not analyze JARFO	12/17/87 1 23 JARGO	3/31/88 1 25 JARHO	 Incomplete
10 JOH # Tape Notes File Name	1/23/87 1 3 Tc Prob, A5 	5/6/87 1 12 No flow, did not analyze 	6/24/87 1 16 JOHBO	3/18/87 1 8 NNOIF, did not digitize 	8/12/87 1 19 JOHDO	4/17/87 No flow, did not analyze 	9/2/87 1 20 Did not analyze 	7/30/87 1 18 JOHGO	 Incomplete 	2/23/87 1 5 ML after 160 JOH20
11 OCO # Tape Notes File Name	12/17/87 12 1,24 	6/17/87 2 16,24 OCOAO	1/13/88 2 7,24 LOC - 50 sec OCOBO	1/6/88 2 2,24 OCOCO	2/29/88 2 18,25 OCODO	4/15/88 1 11 OCOEO	8/21/87 1 19 Close to LOC at descent, lost CO2 OCOFO	7/22/87 1 17 OCOGO	3/2/88 1 22,25 OCOHO	4/7/88 1 26 OCO2O
12 ORR # Tape Notes File Name	3/2/87 1 6 ORRAO	7/29/87 1 18 Tc Prob 	3/16/88 2 10,25 ORRBO	3/25/87 1 9 ORRCO	9/1/87 1 20 ORRDO	8/24/87 1 20 ORREO	11/12/87 1 22 ORRFO	3/25/88 2 22,25 ORRGO	12/9/87 1 23 ORRHO	2/6/87 1 4 ORR20
13 SCO # Tape Notes File Name	3/27/87 1 9 SCOAO	7/13/87 1 17 	3/29/88 3 15,24,25 SCOBO	4/1/87 1 9 SCOCO	9/4/87 1 21 SCODO	2/3/88 2 12,25 SCOEO	10/27/87 1 22 SCOFO	8/31/87 1 20 SCOGO	1/26/88 2 22,24 SCOHO	12/2/87 1 23 SCO2O

RD = Rapid Decompression, ML = Mask Leak, MS = Mask Spec, LOC = Loss of Consciousness

# Subject	1 A-100%	2 A5-100%	3 B-100%D	4 C-93%	5 D-93%D	6 E-90%	7 F-90%	8 G-85%	9 H-85%	10 EONS2
14 SHI	3/13/87		5/29/87	3/27/87		4/30/87				2/18/87
#	1		1	1		1				1
Tape	7		14			11				5
Notes		Incomplete		ML Did not analyze	Incomplete		Incomplete	Incomplete	Incomplete	
File Name	SHIAO		SHIBO			SHIEO				SHI2O
15 SHN	1/25/88	6/3/87	5/27/87	3/30/87	8/3/87	4/28/87	10/28/87	7/10/87	11/30/87	12/4/87
#	2	1	1	1	1	1	1	1	1	1
Tape	6,24	15	13	9	18	11	22	17	23	23
Notes										
File Name	SHNAO		SHNBO	SHNCO	SHNDO	SHNEO	SHNFO	SHNGO	SHNHO	SHN20
6 TED	12/17/87	12/5/87	4/3/87	2/12/88	6/5/87	1/11/88	9/2/87	7/1/87	11/6/87	2/11/87
#	2	1	2	2	1	2	2	1	2	1
Tape	1,23	6	3,10	1,25	15	12,24	17,21	16	19,22	5
Notes			Almost LOC just before descent							
File Name	TEDAO		TEDBO	TEDCO	TEDDO	TEDEO	TEDFO	TEDGO	TEDHO	TED20
17 WRI	3/6/87	4/10/87	6/15/87	3/20/87	8/14/87	12/15/87	9/1/87	7/8/87	9/8/87	10/26/87
#	2	1	1	2	1	2	2	1	1	1
Tape	1,6	10	15	3,8	19	13,23	19,20	17	21	22
Notes	NDFLO,									
File Name	A5	WRIAO	WRIBO	WRICO	WRIDO	WRIEO	WRIFO	WRIGO	WRIHO	WRI20

RD = Rapid Decompression, ML = Mask Leak, MS = Mask Spec, LOC = Loss of Consciousness

7.2 Use of EONS Data for Model Validation.

The various modules which will eventually comprise the integrated ABS model have been individually run under representative conditions to demonstrate their agreement with physiological data from the literature. However, the ABS model cannot be fully validated until the component modules are integrated.

The EONS data presented in Appendix A will be essential in validation of the ability of the ABS to predict the transient flow, pressure, and respiratory gas composition. Bomar[50] has previously demonstrated the use of the EONS data to validate a simple dynamic model of the changes in partial pressure of respiratory gases. Figure 7-2 show the end-tidal oxygen and carbon dioxide partial pressures ($P_{ET}O_2$ and $P_{ET}CO_2$) predicted by his model (dashed continuous lines) and those which occurred during experimental rapid decompression of human subjects breathing 100% and 93% oxygen diluted with air (symbols). There was reasonable agreement between predictions and the data which improved with post-decompression elapsed time. This was true despite the fact that Bomar did not model lung/chest mechanics and he assumed constant rates of oxygen consumption and carbon dioxide production (*i.e.* O_2 uptake and CO_2 excretion were assumed to be independent of the partial pressure gradients across the alveolar membrane). These initial results were encouraging and pointed to specific modifications required to bring the ABS model in closer agreement between the predictions and the experimental data. The Phase II model will include partial pressure dependent alveolar gas transport as well as a dynamic cardiovascular model which will mimic the transient changes in pulmonary blood flow as well as the distribution of blood flow along the vertical axis of the lung. This will enable ventilation perfusion ratio estimates to be made for comparison with data from the literature.[6,51,52,53,54,55,56]

The EONS data will also allow a limited validation of the model for predicting the physiologic effects of PBA at 30 mmHg. Other than the EONS series, there are data from Ernsting[57] on the major effects of pressure breathing on the respiratory and cardiovascular systems. On the other hand, there are only limited data on the effects of pressure breathing on ventilation-perfusion relationships.[58,59] Undoubtedly, the attempt to validate the ABS for higher breathing pressures and its effect on ventilation-perfusion will point to the need for specific data so that experimental protocols can be suggested.

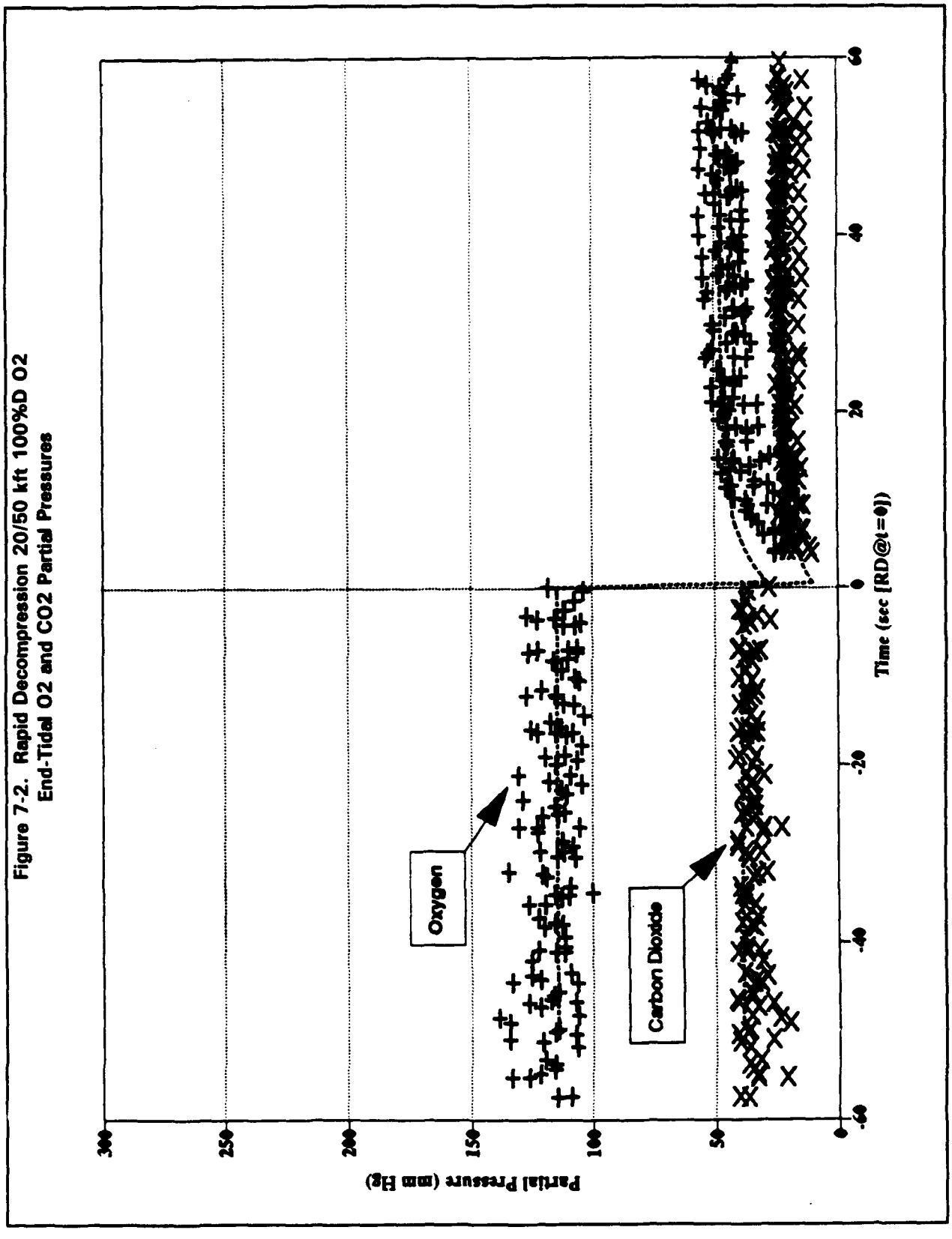

Figure 7-2. Rapid Decompression 20/50 kft 100%D O2
End-Tidal O2 and CO2 Partial Pressures

SECTION 8.0

8.0 Conclusions and Recommendations.

8.1 Conclusions

BRC completed an SBIR Phase I project to study the feasibility of developing a model of the Aviator's Breathing System (ABS). The motivation for the project was the desire to develop a model which could simulate the cardiovascular and respiratory responses to altitude and acceleration stress encountered in high performance military aircraft. Once validated, the model could be employed to integrate existing physiologic knowledge and to estimate the physiologic effects of changes in the environment or the design of aircrew protective equipment.

The Phase I effort was concentrated in developing computer software modules which were capable of simulating the main effects of environmental variables on the breathing system hardware and respiratory and cardiovascular systems. Software modules were developed and tested for simulation of: (1) the flows and pressures within the breathing gas delivery system; (2) the flows, pressures, and respiratory gas distribution within the lung; and (3) the steady-state flows and pressures within the cardiovascular system. Subprograms were also developed to compute altitude-barometric pressure relationships as well as passenger cabin pressures in military aircraft.

In addition to the software development, BRC reviewed and organized the Government furnished data from a series of manned rapid decompressions known as the "EONS Experiments." The data from approximately 170 experimental decompressions were screened for their suitability for use in parameter selection and validation of the respiratory modelling software. The data appears to be highly coherent and fully usable for model validation. The summarized results of the EONS Experiments represent a new physiologic database which is directly applicable to USAF operational scenarios. The respiratory gas composition time histories represent original scientific data suitable for publication and use by the aerospace medicine community independently of their value in the ABS modelling effort.

The work accomplished in Phase I has laid the groundwork for developing an integrated ABS Model in a Phase II SBIR program. BRC has written prototype software modules which form the major building blocks for the Phase II ABS Model. We conclude that the development of an integrated ABS Model is feasible and desirable. We also conclude that there is sufficient existing data for selection of parameters and independent validation of the major components of the Phase II ABS model. However, the complete validation of the combined effects of acceleration, pressure breathing and altitude on the ABS must await new experimental data. Fortunately, the attempt to simulate the physiologic response to combined stressors will explicitly point to missing data and guide the development of experimental protocols to elucidate their significance. The following section outlines the major steps required to create the Phase II model by building on the work accomplished in Phase I.

8.2 Recommendations.

At present, none of the Phase I ABS modules is fully validated. Therefore, prior to their integration, additional development of the Phase I software modules will be required to ensure their ability to independently simulate the physiologic response to changes in their input variables. In addition, the software code and numerical methods for solution of the system equations will be optimized and, where possible, standardized across modules. This will result in more efficient code and ease the process of creating the software interfaces necessary to integrate the Phase I modules into a fully integrated ABS Model. The following sections outline the major work on each software module required before their integration.

8.2.1 Breathing Gas Delivery System.

The breathing gas delivery system is comprised of a source of breathing gas, such as an oxygen supply or a Molecular Sieve Oxygen Concentrator (MSOC), a demand regulator which regulates the flow and pressure of the breathing gas in response to the changes in the ambient pressure and acceleration, and finally an oronasal mask which ensures unidirectional flow of breathing gas and forms a seal to the face of the aviator.

The preferred way to model the breathing gas source would be to model the composition at the demand regulator inlet as a function of the mass flow drawn by the regulator and the ambient pressures. This approach will work for both MSOC based systems or systems based on storage of gaseous or liquid oxygen. Backup oxygen systems such as seat mounted Emergency Oxygen Systems are relatively simple to model. Regulated Back-Up Oxygen Systems, such as those employed with MSOCS can be modelled similarly to the demand regulator, but without dilution of the feed gas.

The demand breathing gas regulator in the present model assumes the flow demanded is supplied at a pressure typical of the functional performance of an ASCC demand regulator. For the Phase II regulator model, it will be necessary to completely parameterize the mass flow-pressure characteristics of the regulator and include G-sensitivity as required. Parameterization of the regulator's performance is preferable to any attempt to model the internal hardware function. Breathing gas regulators are highly nonlinear devices and the effort required to write and solve the equations describing the flow-pressure characteristics of even a simple regulator would be substantial. The regulator model will also include a parametric representation the regulator's supply gas dilution characteristics as function of ambient and outlet pressures. The regulator outlet relief valve will be modelled on the characteristics of a poppit relief valve rather than the ideal relief included in the present model. The mask tube and connector flow-pressure characteristics will employ the isothermal tube flow equations and will allow for turbulent pressure losses.

The oronasal mask model is essentially complete as implemented. The model is based on the functional performance of an ASCC compliant breathing mask. The present model can be modified to change the mask valve area versus pressure function to match an actual mask if

desired. Empirical data can be employed to match the valve characteristics in the model to actual mask flow-pressure data.

8.2.2 Pulmonary Model.

The ventilation pattern in the Pulmonary Model is presently driven by the flows at the mouth (see Figure 5-1). In order to integrate this model with the mask/regulator model, it will be necessary to make pleural and ambient pressures drive the gas flows in the model, i.e. the pressure difference across the chest wall. This will require adding the elastic characteristics of the chest wall to the Pulmonary Model and changing the logic of the numerical solution scheme. This addition will make the model more realistic as pleural pressure changes normally drive gas flow, and in the case of a rapid decompression, changes in the ambient pressure, coupled with the pleural pressure, creates gas flow in the lungs.

Presently the model assumes that the ambient pressure remains 1 atm and that the density of the gas in the lungs remains constant. Obviously, this is not the case when pressure breathing and rapid decompressions are modeled, so the Pulmonary Model will require modification to include the density effects of lung gases which are not presently included. This can be done with relatively little difficulty.

The Pulmonary Model inherently contains the effect of acceleration on ventilation through the G-term in Equation 5-18, but the resulting regional volumes and flow patterns for G-values greater than $+1\ G_z$ have not been studied in detail, and the performance of the model in predicting ventilation patterns in high-G environments will require verification.

In order to integrate the Pulmonary Model with the Cardiovascular Model, the transport of carbon dioxide and oxygen between the alveolar gas and the blood must be included. The model presently tracks the concentration of a single gas in the airways of the four regions, therefore it cannot realistically include the effects of more than one tracer gas species. To accommodate alveolar exchange, the model must be modified to [illegible]nce multiple gas species and to include the transport of oxygen, nitrogen, and carbon di[illegible] throughout the airways and alveoli of each region in the model.

8.2.3 Cardiovascular Model.

The major change required in the cardiovascular model will be to incorporate dynamic response characteristics and add models of the short term physiologic control systems. The steady state effects of acceleration are already implemented in the cardiovascular, but the modifications will be required to include transient changes in flow pressure within the segments. Pressure breathing effects will be implemented by modelling the rise in intrathoracic pressure and its effect on venous return and blood pressure. Methods of modelling pressure garments such as partial pressure garments and anti-G suits must also be added. It should be feasible to model the application of external pressure by manipulation of the tissue pressure (P_{ext}) which is already included in the model. The current version of the

model also runs very slowly with the Runge-Kutta numerical integration algorithm presently employed. Different methods of formulation and solution of the differential equations should be investigated to optimize the speed and stability of the model.

The pulmonary cardiovascular section will be split into four subsections each supplying the corresponding region of the pulmonary model. Local regulation will be simulated as will flow pressure alterations in response to acceleration and pressure breathing.

8.2.4 Integration of Subsystem Modules.

Phase I has created basic modules and a framework for an integrated ABS model. As modern life support systems (LSSs) are substantially integrated, the Phase II model will attempt to include the interaction of the relevant LSS components with the environment and the crew member and other parts of the LSS. Most of these variables will simulated parametrically as inputs to the system to model PBG as well as anti-G suit inflation during pressure breathing for altitude (PBA). Modelling of interfaces will likely be one of the most interesting and most difficult parts of combining the Phase I modules into an integrated ABS model in Phase II. To our knowledge, no one has modelled the interfaces between the life support equipment and the aviator. Just as importantly, with the aid of the ABS Model it should be possible to discover the nature of improvements which would be necessary to correct poor interaction or poor integration between the crew member and the LSS. The integrated ABS Model will be employed to perform parametric studies as an aid to illustrating and understanding the nature of the interactions between the environment, the LSS, and the aviator. A knowledge of the (dynamic) nature of the interaction between the physical and physiologic subsystems will also help guide the Government's research program toward elucidating the physiology necessary to describe the effects of LSS design on aircrew protection.

Once the individual modules are created and validated, they will be integrated into a single software program or an interactive suite of programs. The validation of the integrated software will require more than a recomparison of simulations to the same data employed in the validation of the individual models. Data will be required which describes the effects of a single environmental variable on both the pulmonary and cardiovascular systems. In addition, data on the response of the pulmonary and cardiovascular systems to combined environmental inputs will be required. This phase of the model validation is likely to be the most difficult because of the paucity of data on such effects. Undoubtedly, the attempt to validate the integrated model will point to the need for specific new data.

The design of user and software modules will be a major task of the Phase II development program. The goal will be to design a single software module with a "user friendly" interface which allows easy selection and adjustment of input variables and display of simulation results. It is likely that the display of model time histories will require use of separate graphics programs or spreadsheet models.

Finally, it is recommended that the Phase II development proceed methodically and be spread over a sufficient time to allow for development of new data which may be required. The Phase II models should be developed as independent modules for use independently of the integrated ABS model. This will permit "stand alone" use of the modules or for their further development for projects outside the context of the ABS.

REFERENCES

REFERENCES

1. Hesser, CM; Lind, F. Ventilatory and Occlusion-Pressure Responses to Incremental-Load Exercise. Respir Physiol. 51: 391-401; 1983.

2. Zaleski, PJ; Holden, RD; Hiott, BF. Biomedical Aspects of Oxygen Regulator Performance: I. Static Characteristics. Aviat Space Environ Med. 47(5): 485-494; 1976.

3. Zaleski, PJ; Holden, RD. Biomedical Aspects of Oxygen Regulator Performance: I. Dynamic Characteristics. Aviat Space Environ Med. 47(5): 495-502; 1976.

4. Holden, RD; Bomar, JB; O'Connor, RB; Wright, CS; Nesthus, TE. Acceptability of Standard USAF Breathing Gear at High Altitude. Proceedings of the 25th Annual SAFE Symposium. 166-170; 1987 November.

5. Ernsting, J. The Effects of Resistance to Respiration in Man - A Review of the Literature. Royal Air Force Institute of Aviation Medicine; IAM Report #112; 1959 January.

6. Tedor, JB; Clink, JP. Man Rating the B-1B Molecular Sieve Oxygen Generation System. Human Systems Division (AFSC), Brooks AFB, TX. USAFSAM-TR-87-4. 1987 August.

7. Wright, CS; Clink, JP. A Study of A-37 Aircraft Oxygen Consumption. Human Systems Division (AFSC), Brooks AFB, TX. USAFSAM-TR-88-1. 1988 May.

8. Byrne, JC; McIlwain-Axten, CJ. An Analytical Model of the Aircrew Oxygen Breathing System. SAFE Journal. 22(6): 8-14; 1992.

9. See, for example: The Handbook of Respiratory Physiology for useful models of steady state gas exchange and Aviation Medicine, 2nd Edition; Ernsting and King, Ed.; London: Butterworths; 1988; or Fundamentals of Aerospace Medicine; R.L. DeHart, Ed.; Philadelphia, PA: Lea & Febiger; 1985; for applications of steady state models to the aviation environment.

10. West, JB. Respiratory Physiology - the essentials, 3rd Ed. Baltimore, MD: Williams & Wilkins; 1985.

11. Heijmans, JL; Bert, JL; Pinker, KL. Digital Simulation of Pulmonary Microvascular Exchange. Comput Biol Med. 16(2): 69-90; 1986 February.

12. Kapitan, KS; Hempleman, SC. Computer Simulation of Mammalian Gas-Exchange. Comput Biol Med. 16(2): 91-101; 1986 February.

13. Petrini, MF. Distribution of Ventilation and Perfusion: A Teaching Model. Comput Biol Med. 16(6): 431-444; 1986 June.

14. Sherrill, DL; Dietrich, BH; Swanson, GD. On the Estimation of Pulmonary Blood Flow from CO_2 Production Time Series. Computers and Biomedical Research. 21: 503-511; 1988.

15. Granger, WM; Miller, DA; Ehrhart, IC; Hofman, WF. The Effect of Blood Flow and Diffusion Impairment on Pulmonary Gas Exchange: A Computer Model. Computers and Biomedical Research. 20:497-506; 1987.

16. Peterman, BF; Longtin, A. Multicompartment Model of Lung Dynamics. Computers and Biomedical Research. 17: 580-589; 1984.

17. Rosburgh, HL; Ernsting, J. The Physiology of Pressure Suits. Aviation Medicine. 260-271; 1957 June.

18. White, RJ; Croston, RC; Fitzjerrell, DG. Cardiovascular Modelling: Simulating the Human Cardiovascular Response to Exercise, Lower Body Negative Pressure, Zero Gravity and Clinical Conditions. Adv Cardiovasc Phys. 5(Part I): 195-229; 1983.

19. Jaron, D; Moore, TW; Bai, J. Cardiovascular Response to Acceleration Stress: A Computer Simulation. Proceedings of the IEEE. 76(6): 700-707; 1988.

20. Jaron, D; Moore, TW; Vieyres, P. A Cardiovascular Model of G-Stress Effects: Preliminary Studies with Positive Pressure Breathing. IN: High Altitude and High Acceleration: Protection for Military Aircrew. Neuilly-sur-Seine, France: Advisory Group for Aerospace Research and Development (AGARD). 7 pp.; 1991 October.

21. Jaron, D; Moore, TW; Chu C-L. A Cardiovascular Model for Studying Impairment of Cerebral Function During $+G_z$ Stress. Aviat Space Environ Med. 55(1): 24-31; 1984.

22. Rideout, VC; Dick, DE. Difference-Differential Equations for Fluid Flow in Distensible Tubes. IEEE Trans. Bio-Med Engr. 14(4): 171-177; 1967.

23. Snyder, MF; Rideout, VC. Computer Simulation of the Venous Circulation. IEEE Trans. Bio-Med Engr. 16(4): 325-334; 1969.

24. Avula, XJR; Ostreicher, HL. Mathematical Model of the Cardiovascular System Under Acceleration Stress. Aviat Space Environ Med. 49(1): 279-286; 1978.

25. Womersley, JR. An elastic tube theory of pulse transmission and oscillatory flow in mammalian arteries. Wright Air Development Report WADC-TR-56-614. 1957.

26. Human-PC, available from Dr. James E. Randall, Indiana University School of Medicine, Bloomington, Indiana 47405.

27. Air Standard Agreement 61/21. Air Standardization and Coordinating Committee. Washington, DC. 1982 August 18.

28. Bomar, J. Personal Notes. USAF School of Aerospace Medicine. 1981.

29. Matalon, S; Dashkoff, N; Nesarajah, MS; Klocke, FJ; Farhi, LE. Effects of hyperventilation on pulmonary blood flow and recirculation time of humans. J Appl Physiol. 52(5): 1161-1166; 1982.

30. Weibel, ER. Morphometry of the Human Lungs. Berlin: Springer-Verlag; 1963.

31. Pedley, TJ; Schroter, RC; Sudlow, MF. The Prediction of Pressure Drop and Variation of Resistance within the Human Bronchial Airways. Respir Physiol. 9(3): 387-403; 1970.

32. Hughes, JMB; Rosenzweig, DY; Kivitz, PB. Site of airway closure in excised dog lungs: Histologic demonstration. J Appl Physiol. 29: 340-344; 1970.

33. Engel, LA; Grassino, A; Anthonisen, NR. Demonstration of airway closure in man. J Appl Physiol. 38(6): 1117-1125; 1975.

34. Sobin, SS; Tremer, HM; Fung, YC. The morphometric basis of the sheet-flow concept of the pulmonary alveolar microcirculation in the cat. Circ Res. 26: 397-414; 1970.

35. Fung, YC; Sobin, SS. Elasticity of the pulmonary alveolar sheet. Circ Res. 30: 451-469; 1972.

36. Sobin, SS; Fung, YC; Tremer, HM; Rosenquist, TH. Elasticity of the pulmonary alveolar microvascular sheet in the cat. Circ Res. 30: 440-450; 1972.

37. Sasaki, H; Takishima, T; Sasaki, T. Influence of lung parenchyma on dynamic bronchial collapsibility of excised dog lungs. J Appl Physiol. 42(5): 699-705; 1977.

38. Sasaki, H; Hoppin Jr, FG; Takishima, T. Peribronchial pressure in excised dog lungs. J Appl Physiol. 45(6): 858-869; 1978.

39. Hughes, JMB; Hoppin Jr, FG; Mead, J. Effect of lung inflation on bronchial length and diameter in excised lungs. J Appl Physiol. 32(1): 25-35; 1972.

40. Shapiro, AG. Steady flow in collapsible tubes. J Biomechanical Eng. 126-147: 1977.

41. Milic-Emili, J; Henderson, JAM; Dolovich, MB; Trop, D; Kaneko, K. Regional distribution of inspired gas in the lung. J Appl Physiol. 21: 749-759; 1966.

42. Robertson, PC; Anthonisen, NR; Ross, D. Effect of inspiratory flow rate on regional distribution of inspired gas. J Appl Physiol. 26(4): 438-443; 1969.

43. Millette, B; Robertson, PC; Ross, WRD; Anthonisen, NR. Effect of expiratory flow rate on emptying of lung regions. J Appl Physiol. 27(5): 587-591; 1969.

44. Hansen, JE; Ampaya, EP. Human air space shapes, sizes, areas and volumes. J Appl Physiol. 38(6): 990-995; 1975.

45. Fung, YC. Biomechanics. New York: Springer-Verlag; 1993.

46. Bergel, DH. The Dynamic Elastic Properties of the Arterial Wall. J Physiol. 156: 458-469; 1961.

47. Burton, AC. Physiology and Biophysics of the Circulation. Chicago, IL: Year Book Medical Publishers, Inc.; 1965.

48. Guyton, AC. Textbook of Medical Physiology. 7th Ed. Philadelphia, PA: W.B. Saunders; 1985.

49. Schiesser, WE. The Numerical Method of Lines. San Diego: Academic Press Inc.; 1991.

50. Bomar, JB. "New Developments in Altitude Protection." Presented in Panel Session Entitled "Perspectives on Hypoxia." Scientific Program. May 1990. Abstract No. 353: A65.

51. DuBois, AB; Brody, AW; Lewis, DH; Burgess Jr, BF. Oscillation Mechanics of Lungs and Chest in Man. J Appl Physiol. 8: 587-594; 1956 May.

52. Ernsting, J. The Genesis and Reduction of Resistance to Breathing in Aircraft Oxygen Delivery Systems. Royal Air Force Institute of Aviation Medicine, Farnborough, Hants, England GU14 6SZ. 1-4.

53. Fry, DL; Hyatt, RE; McCall, CB; Mallos, AJ. Evaluation of Three Types of Respiratory Flowmeters. J Appl Physiol. 10(2): 210-214; 1957.

54. Landervik, B; Dahlback, G. Man rating of the Anti-G protection in a human centrifuge of the Tactical Flight Combat Suit (TRCS), the EROS oxygen regulator/anti-G valve with Swedish JAS 39 test pilots (11 Appendix). Forsvarets Materielverk Test Report. 1-35; 1991.

55. Taylor, SJ. Estimating the Variances of Autocorrelations Calculated from Financial Time Series. Appl Statist. 33(3): 300-308; 1984.

56. Tesch, PA. Anaerobic Testing - Research Basis. NSCA Journal (National Strength & Conditioning Assn.); 66-69; 1984 October-November.

57. Engel, LA; Menkes, H; Wood, LDH; Utz, G; Joubert, J; Macklem, PT. Gas mixing during breath holding studied by intrapulmonary gas sampling. J Appl Physiol. 35(1): 9-17; 1973.

58. Bhansali, PV; Irvin, CG; Dempsey, JA; Bush, R; Webster, JG. Human pulmonary resistance: effect of frequency and gas physical properties. J Appl Physiol. 47(1): 161-168; 1979.

59. Montgomery, LD; Hanish, HM; Burns, JW. A System to Measure Lower body Volume Changes During Rapid Onset High-G Acceleration. Aviat Space Environ Med. 59: 1098-1102; 1988.

☆U.S. GOVERNMENT PRINTING OFFICE: 1994 - 560-051/00010